



**HAL**  
open science

## Geomagnetic Secular variation in the Cretaceous Normal Superchron and in the Jurassic

Andrew J. Biggin, Douwe J.J. van Hinsbergen, Cor G. Langereis, Gijs B.  
Straathof, Martijn H.L. Deenen

► **To cite this version:**

Andrew J. Biggin, Douwe J.J. van Hinsbergen, Cor G. Langereis, Gijs B. Straathof, Martijn H.L. Deenen. Geomagnetic Secular variation in the Cretaceous Normal Superchron and in the Jurassic. *Physics of the Earth and Planetary Interiors*, 2008, 169 (1-4), pp.3. 10.1016/j.pepi.2008.07.004 . hal-00532159

**HAL Id: hal-00532159**

**<https://hal.science/hal-00532159>**

Submitted on 4 Nov 2010

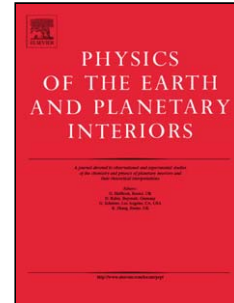
**HAL** is a multi-disciplinary open access archive for the deposit and dissemination of scientific research documents, whether they are published or not. The documents may come from teaching and research institutions in France or abroad, or from public or private research centers.

L'archive ouverte pluridisciplinaire **HAL**, est destinée au dépôt et à la diffusion de documents scientifiques de niveau recherche, publiés ou non, émanant des établissements d'enseignement et de recherche français ou étrangers, des laboratoires publics ou privés.

## Accepted Manuscript

Title: Geomagnetic Secular variation in the Cretaceous Normal Superchron and in the Jurassic

Authors: Andrew J. Biggin, Douwe J.J. van Hinsbergen, Cor G. Langereis, Gijs B. Straathof, Martijn H.L. Deenen



PII: S0031-9201(08)00166-0  
DOI: doi:10.1016/j.pepi.2008.07.004  
Reference: PEPI 4997

To appear in: *Physics of the Earth and Planetary Interiors*

Received date: 5-2-2008  
Revised date: 4-7-2008  
Accepted date: 5-7-2008

Please cite this article as: Biggin, A.J., van Hinsbergen, D.J.J., Langereis, C.G., Straathof, G.B., Deenen, M.H.L., Geomagnetic Secular variation in the Cretaceous Normal Superchron and in the Jurassic, *Physics of the Earth and Planetary Interiors* (2007), doi:10.1016/j.pepi.2008.07.004

This is a PDF file of an unedited manuscript that has been accepted for publication. As a service to our customers we are providing this early version of the manuscript. The manuscript will undergo copyediting, typesetting, and review of the resulting proof before it is published in its final form. Please note that during the production process errors may be discovered which could affect the content, and all legal disclaimers that apply to the journal pertain.

1 **Geomagnetic Secular variation in the Cretaceous Normal Superchron and in the**  
2 **Jurassic**

3

4 Andrew J. Biggin<sup>1\*</sup>, Douwe J.J. van Hinsbergen<sup>1,2</sup>, Cor G. Langereis<sup>1</sup>, Gijs B.  
5 Straathof<sup>1,2†</sup>, Martijn H.L. Deenen<sup>1</sup>

6

7 *1. Paleomagnetic Laboratory 'Fort Hoofddijk', Utrecht University, Budapestlaan 17,*  
8 *3584 CD Utrecht, The Netherlands*

9

10 *2. Department of Geology, University of Leicester, University Road, LE1 7RH*  
11 *Leicester, UK*

12

13 *\*Corresponding author. Tel. +31.30.253.5246, e-mail: biggin@geo.uu.nl*

14

15 **Abstract**

16 It is now widely thought that geomagnetic polarity reversals occur spontaneously as a  
17 result of normal dynamo action rather than being externally triggered. If this is the case,  
18 then it may well be that periods of time in which the geomagnetic reversal frequency was  
19 dramatically different were characterised by different styles of secular variation. Two  
20 such periods were the Cretaceous Normal Superchron (CNS - 84-125 Ma) when the field  
21 was dominantly of a single polarity for 40 Myr and the Jurassic period (145-200 Ma)  
22 when reversals occurred at an average rate of as much as 4.6 Myr<sup>-1</sup>. Here we analyse a  
23 database of new and published palaeomagnetic directions from lavas emplaced during

†Now at: School of Geosciences, Grant Institute, West Mains Road, University of Edinburgh, UK

1 these periods in order to obtain first-order descriptions of the palaeosecular variation  
2 (PSV) during these times. We then compare these records with one another and with that  
3 produced for the period 0-5 Ma (with average reversal frequency  $4.0 \text{ Myr}^{-1}$ ). Our results  
4 are more equivocal than those obtained in a previous similar study (McFadden et al.,  
5 1991, Reversals of the Earths Magnetic-Field and Temporal Variations of the Dynamo  
6 Families. *J. Geophys. Res.* 96, 3923-3933). We demonstrate that this is probably a result  
7 of the previous study being affected by an artefact of their correction for within-site  
8 scatter. The usefulness of our Jurassic record is severely limited by the restricted  
9 palaeolatitudinal span of the available data. However, our record for the CNS is sufficient  
10 to allow us to conclude that it was likely that secular variation then was different from  
11 that in the 0-5 Ma period. This supports the hypothesis of a link between PSV and  
12 reversal frequency and therefore endorses PSV analysis as a first-order tool for  
13 determining geomagnetic stability in the past.

14

15 **Keywords:** geomagnetic field; palaeomagnetism; secular variation; Cretaceous; Jurassic;  
16 superchron

17

## 18 **1. Introduction**

19 The Secular Variation (SV) of the geomagnetic field is the variation (on timescales of  
20 hundreds to thousands of years) that arises internally from the dynamo action which is  
21 responsible for generating the field. Numerical models of the geodynamo (e.g.  
22 Glatzmaier and Roberts, 1995) which exhibit SV may also spontaneously exhibit more  
23 dramatic ‘excursions’ and full polarity reversals similar to those observed in the

1 palaeomagnetic record. Partly as a result of these simulations, it is now widely thought  
2 that excursions and reversal transitions are natural outgrowths of SV (Gubbins, 1999) and  
3 not externally triggered by e.g. boundary layer instabilities as has been previously  
4 considered (e.g. McFadden and Merrill, 1993).

5

6 Magnetostratigraphy has provided unambiguous evidence that the propensity of the  
7 geomagnetic field to reverse its polarity has varied over timescales of  $10^7$  to  $10^8$  years  
8 (e.g. Opdyke and Channell, 1996). These are much longer than the timescales typically  
9 associated with the core and are likely forced through mantle processes changing the total  
10 heat flux across the core-mantle boundary and/or its lateral distribution (Gubbins, 1994).  
11 Numerous attempts have been made to tie in these variations in reversal frequency to  
12 observations of the long-term average geomagnetic palaeointensity (e.g. Biggin and  
13 Thomas, 2003; Prevot et al., 1990; Tarduno et al., 2001; Tarduno et al., 2002; Tauxe and  
14 Staudigel, 2004; Thomas et al., 2000) as well as geological processes observed at the  
15 Earth's surface (e.g. Courtillot and Olson, 2007; Larson and Olson, 1991). If reversals are  
16 intrinsic outgrowths of 'normal' SV then we may expect that records of Palaeosecular  
17 Variation (PSV) should also display such long timescale variations in keeping with  
18 changes in mean reversal frequency. This study aims to test this hypothesis using new  
19 data and a different analytical approach to that used by McFadden et al. (1991).

20

21 Palaeomagnetic records from sedimentary sections (e.g. Tauxe & Hartl, 1997) can  
22 provide continuous full-vector records of PSV. However, all but the most rapidly  
23 deposited sediments will tend to average out the variation to some degree that may be

1 difficult to quantify. Conversely, palaeomagnetic directions measured from lava samples  
2 provide an essentially instantaneous spot reading of the geomagnetic field. This, together  
3 with the fact that the ‘within-site statistics’ measurable from lavas allows correction for  
4 measurement errors implies that lavas provide potentially more reliable data for statistical  
5 analyses of PSV than do sedimentary rocks. One potential drawback of Palaeosecular  
6 Variation of Lavas (PSVL) studies is that rapid bursts of volcanic activity can result in  
7 under-representation of PSV (e.g. Knight et al., 2004). However, this potential problem  
8 can be detected by careful analysis of the data (see section 2 of this study).

9

10 PSV analyses are most commonly performed by taking Virtual Geomagnetic Poles  
11 (VGPs) from numerous lavas and plotting their angular dispersion against the  
12 (palaeo)latitude of the source rocks on a *VGP dispersion curve*. McFadden et al. (1991)  
13 reported clear and significant differences in VGP dispersion curves from time periods  
14 within the last 195 Myr with different average reversal frequencies. In particular, they  
15 found that during times of low reversal frequency, VGP dispersion tended to be lower at  
16 low palaeolatitudes than during times of higher reversal frequencies and also that this  
17 dispersion increased much more with increasing palaeolatitude in the former than in the  
18 latter periods. These observations imply that normal SV is intrinsically linked to reversal  
19 frequency and also suggest that PSVL can be used as a tool, independent of  
20 magnetostratigraphy, to ascertain dynamo stability at other times in Earth’s history.

21

22 McFadden et al’s findings were based on a database compiled 25 years ago (Lee, 1983)  
23 which was split up into bins based on the palaeolatitude and age of the VGPs. No details

1 of the individual studies providing the data were given and more recent PSVL studies  
2 have cast doubt on the reliability of some of the findings. In addition to reporting a  
3 detailed full-vector palaeomagnetic analysis of mid-Cretaceous Arctic lavas, Tarduno et al.  
4 (2002) produced a VGP dispersion curve for the Cretaceous Normal Superchron and  
5 found that it was not as steep as that observed for the same period by McFadden et al.  
6 This difference was probably, at least partly, a result of the more recent study using far  
7 more exacting selection criteria than the earlier work. The present study supersedes the  
8 PSV analysis of Tarduno et al. because we use a substantially larger overall dataset and  
9 pay special attention to the within-site statistics of these data.

10

11 Very recently, Johnson et al. (2008) performed the most detailed and rigorous PSVL  
12 study yet using data from lavas formed in the last 5 Myr. Their data was unquestionably  
13 more reliable than that available to previous studies of the same period (e.g. McElhinny  
14 and McFadden, 1997; McFadden et al., 1988) and, interestingly, it produced a VGP  
15 dispersion curve that was significantly flatter in shape than the curves the older studies  
16 had produced. Furthermore, they demonstrated using simulated data that latitudinal  
17 dependence of VGP dispersion can be introduced as an artefact of poor quality data.

18

19 The Glatzmaier-Roberts numerical geodynamo model (Glatzmaier et al., 1999) operating  
20 in different stability regimes produces VGP dispersion curves with different shapes  
21 (figure 1). Specifically, the mean VGP dispersion curve produced by their highly stable  
22 ‘superchron-like’ Model E is lower than that produced by their Model G which has a  
23 reversal frequency closer to the present-day field. Furthermore, there is a broad tendency

1 for the standard deviation of the VGP dispersion (shown in figure 1 as error bars) to  
2 increase with its mean value. Consequently, the Model E curve shown in figure 1a  
3 indicates that the pattern of PSV (as defined by VGP dispersion produced by sites  
4 positioned along a complete circle of latitude) was less variable in time than that for  
5 Model G.

6

7 In this study we will use the PSVL technique to examine if SV is different in periods of  
8 dramatically different reversal frequency. Such a connection is suggested by numerical  
9 models and the empirical study of McFadden et al. (1991), and might also be intuitively  
10 expected.

11

12 In section 2 we present the analytical techniques we used in this study and in section 3 we  
13 look in detail at the effects that low quality data can have on a PSVL study. This will  
14 serve the purpose of guiding future studies.

15

16 In section 4 we will introduce the datasets that were used in this analysis. These were  
17 taken from rocks from a total of 11 localities emplaced in the CNS and rocks from 17  
18 localities from the Jurassic period. These two periods were chosen because the analysis of  
19 McFadden et al. (1991) found that data in the time windows 80-120 Ma and 120-195 Ma  
20 displayed PSV behaviour at the extreme ends of the spectrum of behaviour they observed  
21 across the entire period 0-195 Ma.

22

1 There is some controversy over the precise date of the onset of the CNS (see e.g. Gong et  
2 al., 2008 for a discussion) but we will take here the period 84-125 Ma defined by  
3 Gradstein et al. (2004). The superchron (C34n in the geomagnetic polarity timescale)  
4 may contain up to three brief reversed sub-chrons (Ogg and Smith, 2004) implying a  
5 maximum reversal frequency of  $0.15 \text{ Myr}^{-1}$ . The average reversal frequency for the  
6 Jurassic period (145-200 Ma) is less well-constrained since the period denoted by chrons  
7 M25 to M36 suggest many more reversals in the deep tow (MMA - marine magnetic  
8 anomaly) record than are indicated in magnetostratigraphic outcrop sections. If each of  
9 the inferred reversals in the MMA record is accepted then the average frequency across  
10 the whole period is  $4.6 \text{ Myr}^{-1}$  but this value could be reduced to as low as  $3.1 \text{ Myr}^{-1}$  if  
11 only reversals evident in the outcrop sections are to be trusted. It should also be noted that  
12 our knowledge of the reversal record during the period 190-200 Ma is rather poorly-  
13 constrained (Ogg, 2004).

14

15 In section 5 we compare the VGP dispersion curves produced by the data from the CNS  
16 and Jurassic period and in section 6, we compare these curves with the Johnson et al.  
17 curve for the last 5 Myr and discuss all of our findings.

18

## 19 **2. Methodology**

20 We group palaeomagnetic data into *datasets*, each one of which consists of a collection of  
21  $N$  VGPs from rocks of similar age and from the same geographic region (frequently the  
22 same formation). Each one of these VGPs is produced from a single palaeomagnetic  
23 sampling site equating to a single rock unit (lava, tuff, or high-level intrusion) and we are

1 interested in using their angular dispersion as a measure of PSV. This dispersion will be  
 2 partly caused by the geomagnetic secular variation, and partly by random errors  
 3 associated with the sampling and measuring process. It is desirable to remove the latter  
 4 source of dispersion so that the accuracy of the estimate of the dispersion caused by the  
 5 SV is improved. The angular dispersion of VGPs from  $N$  units due to SV ( $S_B$ ) is  
 6 calculated thus:

$$7 \quad S_B = \left[ \frac{1}{N-1} \sum_{i=1}^N \left( \Delta_i^2 - \frac{S_{W_i}^2}{n_i} \right) \right]^{1/2} \quad (i = 1, \dots, N) \quad (1)$$

8 where  $\Delta_i$  gives the angular distance of the  $i$ th VGP from the geographic pole or mean  
 9 VGP.  $S_{W_i}$  is the within-site dispersion associated with each VGP which must be estimated  
 10 from the scatter observed between the  $n_i$  individual sample directions.  $S_{W_i}$  and  $n_i$  will be  
 11 abbreviated to  $S_W$  and  $n$  from hereon. To calculate  $S_W$ , first the known estimate of the  
 12 precision parameter,  $k$  is (approximately) translated from direction to pole-space using  
 13 equation (2) from Cox (1970) which makes the reasonable assumption of a Fisherian  
 14 distribution (Fisher, 1953) of within-site directions:

$$15 \quad K = k \left( \frac{1}{8} (5 + 18 \sin^2 \lambda + 9 \sin^4 \lambda) \right)^{-1} \quad (2)$$

16 where  $\lambda$  is the palaeolatitude of the sampling site and  $K$  and  $k$  are the within-site precision  
 17 parameters of the distribution in pole and direction space respectively. The within-site  
 18 dispersion is then approximated by:

$$19 \quad S_W = 81 / \sqrt{K} \quad (3)$$

20 Regardless of whether or not geomagnetic excursions and reversal transitions are purely  
 21 outgrowths of 'normal' SV, their presence in a complete description of the time-averaged

1 field is warranted. That said, the proportion of time the field spends in such a state is  
2 rather small and measurements of  $S_B$  are strongly influenced by ‘outlier’ VGPs (because  
3 it is sensitive to  $\Delta i^2$ . Therefore, we consider it desirable to exclude definitely excursions  
4 data (as well as outliers produced by measurement or recording errors) and to focus on  
5 the dispersion of VGPs produced by the field undergoing SV away from times of  
6 excursions and reversals. To do this, it is necessary to apply some threshold for  $\Delta i$  of  
7 VGPs in a dataset. There are two common approaches to obtaining this maximum cutoff  
8 value and both will be employed here. The first is to apply some arbitrary fixed cutoff  
9 value; when we employ this approach, we choose  $45^\circ$  as this is intermediate between the  
10 extremes chosen by previous studies and is also the value chosen by Johnson et al. (2008)  
11 for their analysis of the 0-5 Ma period. The second is to make the (reasonable)  
12 assumption that the distribution of VGPs is Fisherian (Fisher, 1953) and to use the  
13 iterative process defined by Vandamme (1994) to obtain an optimum cutoff angle,  
14 variable with palaeolatitude, from the dataset itself.

15

16 Some PSVL studies (e.g. McFadden et al., 1991) use plate reconstructions to relocate  
17 palaeomagnetic sampling sites to their position at the time the lavas were emplaced. The  
18 value of  $\Delta i$  in equation (1) is then calculated as the angular distance of the VGP from the  
19 ‘geographic’ pole. However, these plate reconstructions may themselves be based largely  
20 on the results of palaeomagnetic studies or else on the doubtful (Tarduno et al., 2003)  
21 fixed hotspot assumption. Therefore, in this study, we prefer to use the palaeomagnetic  
22 data to define the geographic pole directly based on the Geocentric Axial Dipole (GAD)  
23 assumption. We therefore take the mean of the VGPs from the  $N$  sites in a dataset as the

1 geographic pole and measure  $\Delta_i$  from this mean pole. We also use the inclination of the  
2 mean direction to obtain our measurement of  $\lambda$ , the palaeolatitude of the dataset. The  
3 accuracy of this approach for different sizes of datasets (i.e. different values of  $N$ ) is  
4 examined in section 3.2.

5

6 Implicit to the study of PSV using measurements of VGP dispersion is the assumption  
7 that the geomagnetic field activity is sufficiently represented in the datasets. This requires  
8 a sufficiently large dataset of VGPs spanning a sufficient length of time (ideally at least  
9 several tens or hundreds of thousands of years, Merrill and McFadden, 2003). A potential  
10 problem of using data from lavas is that they can be emplaced in rapid bursts of volcanic  
11 activity which last only a short amount of time. A symptom of a sequence of lavas under-  
12 representing PSV is that the VGP positions from each flow display some serial  
13 correlation as the directions tracked the drift of the geomagnetic pole. However, while a  
14 lack of serial correlation in a large dataset implies that PSV must be well-represented, the  
15 converse is not true: the presence of serial correlation, particularly in a large dataset, does  
16 not make an under-representation of the time-averaged field indubitable.

17

18 In the present study, it was deemed useful to have some quantitative non-parametric test  
19 for serial correlation in our datasets. For this we introduce a Non-Random-Ordering  
20 (NRO) factor which is calculated as follows:

- 21 1. Input the dataset of palaeomagnetic directions in stratigraphic order if known.
- 22 2. Calculate the angular distance  $\Delta_{i(i+1)}$  between the palaeomagnetic direction of each  
23 flow and its successor.

1 3.Sum these to produce  $\Sigma\Delta_{i(i+1)}$

2 4.Randomise the order of the magnetic directions and repeat steps 2 and 3.

3 5.Repeat step 4 10,000 times and rank the values of  $\Sigma\Delta_{i(i+1)}$  produced.

4

5 The position of the original  $\Sigma\Delta_{i(i+1)}$  amongst the 10,000 randomised values is then  
6 indicative of the degree of ordering in the original dataset. Specifically, its rank divided  
7 by 10,000 is the *NRO factor* we will use which is the probability of this order being non-  
8 random. Consequently, the serial correlation is significant at the 95% confidence level if  
9 the NRO factor exceeds 0.95. This is essentially the same procedure for detecting serial  
10 correlation as that outlined by Watson & Beran (1967) but does not require the  
11 assumption that the  $\Sigma\Delta_{i(i+1)}$  values are normally distributed.

12

13 The NRO factor is equally effective at detecting clusters of similar magnetic directions as  
14 it is at detecting progressive serial correlation. This is useful because many  
15 palaeomagnetic studies do not provide an explicit stratigraphy but do group sites by  
16 sampling localities which may produce related directions. In this study, by inputting the  
17 data in an order which reflects the geographic distribution of the sampling sites, it was  
18 still possible to provide some test for potential under-representation of SV in several of  
19 the studies which did not provide an explicit stratigraphic relationship.

20

21 The NRO factor should, in most cases, indicate where bursts of extrusive activity could  
22 lead to the over-representation of short periods of SV. However, in this study we only  
23 seek to identify this problem and discuss its significance and not to correct for it. Very

1 similar directions from consecutive lavas are sometimes averaged by researchers (e.g.  
2 Knight et al., 2004) but this is not something that we will subject either our own or other  
3 published data to in this study. The reasons for this are, firstly, that there is no objective  
4 way of determining precisely how similar two or more directions should be in order that  
5 they are averaged, and secondly that, as will be explained in section 4.2, it is largely  
6 unnecessary for the purposes of this study. This notwithstanding, future palaeomagnetic  
7 studies should of course always design their sampling strategy with the aim of  
8 maximising the likelihood of averaging SV.

9

10 The phenomenological Model G of McFadden et al.(1988) is used to describe the shapes  
11 of VGP dispersion curves. This model describes  $S_B$  as a function of (palaeo)latitude ( $\lambda$ )  
12 using two shape parameters  $a$ , and  $b$ :

$$13 \quad S_B = \sqrt{a^2 + (b\lambda)^2} \quad (4)$$

14 In this study, the values of  $a$  and  $b$  are chosen to minimise the sum of the squares of the  
15 deviation of the curve from the data. Model G was produced based on observations of the  
16 recent field (IGRF65); the  $a$  parameter is argued to represent variations in the equatorially  
17 asymmetric spherical harmonic terms of the field and the  $b$  parameter represents  
18 variations in the equatorially symmetric terms. We use it in this study to allow  
19 comparisons to be made with the results of McFadden et al. (1991).

20

21 For the plots where we bin the  $S_B$  data by from the datasets by palaeolatitude, we will also  
22 use the same approach as McFadden et al. (1991) where the mean dispersion  $S_\lambda$  of a bin is  
23 given by:

$$1 \quad S_{\lambda} = \bar{S}_B = \left[ \frac{\sum S_B^2 (N-1)}{(\sum N) - 1} \right]^{1/2} \quad (5)$$

2 and its palaeolatitude is the simple arithmetic mean of the binned datasets.

3

4 In sections 3 and 6 we will use simulated datasets to test various different aspects of the  
5 PSVL analysis. These datasets are all generated in the same way.

- 6 1. A number  $N$  of VGPs are randomly generated from a Fisher distribution with  
7 mean position at the geographic north pole and with precision parameter  $K$   
8 calculated (equation 3) from the ‘true’ (input) angular dispersion,  $S_B$ .
- 9 2. Each of these VGPs is converted into a corresponding direction at latitude  $\lambda$ .
- 10 3. Each one of these then forms the centre of a Fisher distribution (in direction  
11 space) with (input) precision parameter  $\kappa$  from which  $n$  directions can be drawn at  
12 random from.

13 The resulting simulated dataset realistically combines the dispersion due to both secular  
14 variation and within-site random errors.

15

### 16 **3. The potential for bias in PSVL studies**

#### 17 *3.1 The effects of $n$ and $k$ on VGP dispersions*

18 The conclusions of PSV studies may potentially be strongly biased by the quality of data  
19 used in the analysis. Johnson et al.(2008) provided evidence that the strong latitudinal  
20 dependence of VGP dispersion observed from lavas of the last 5 Myr by McElhinny and  
21 McFadden (1997) may, at least in part, be an artefact of the low technical quality of the  
22 data that were used.

1

2 Since the conversion of magnetic directions into VGPs uses the (palaeo)latitude of the  
3 sampling site, latitudinally independent within-site dispersion of mean directions will  
4 translate directly into a latitudinal-dependent dispersion of VGPs. The  $S_W$  correction built  
5 into equation (1) can remove this artefact but to work properly it requires that  $n$ , the  
6 number of samples used to produce the mean direction, is sufficiently large so that the  
7 estimated precision parameter,  $k$  is a good estimate for the actual precision parameter,  $\kappa$ .

8

9 In figure 2 we show the results of several simulations of PSV studies. In all cases, the  
10 dispersion of VGPs due to geomagnetic SV is Fisherian, constant with latitude and  $15^\circ$ .  
11 All the deviations from  $S_B = 15^\circ$  are entirely due to artefacts introduced by the measuring  
12 process. A number of interesting observations can be made from these plots. Figure 2a  
13 shows that a large amount of within-site scatter coupled with no  $S_W$  correction being  
14 applied causes a strong positive latitudinal dependence of VGP dispersion to be  
15 introduced. This is largely removed if one incorporates the  $S_W$  correction but, because the  
16  $k$  values of the site mean directions are poorly constrained by the low  $n$ , this introduces its  
17 own artefact (in this case a weak negative latitudinal dependence of VGP dispersion on  
18 latitude). Applying a minimum criterion for the apparent  $k$  value produces an artefact  
19 intermediate between the two described above.

20

21 Figure 2b shows that a dataset with high  $n$  but low  $\kappa$  can still produce a positive  
22 latitudinal dependence of VGP dispersion if a  $S_W$  correction is not applied. However,  
23 since the  $k$  values are now well constrained, the  $S_W$  correction now works reasonably

1 well. Figures 2c and 2d indicate that low within-site errors, even when coupled to a low  $n$   
2 and not corrected for, do not lead to significant artefacts being introduced.

3

4 When the data used in the present study (see section 4) are combined, the total number  
5  $\Sigma N$  of site mean directions from lavas where  $k$  was likely to be well-defined (i.e those  
6 with  $n \geq 5$ ) was 498. The median  $k$  value for these mean directions was 182.  
7 Consequently, we choose  $\kappa = 182$  for the rest of the simulations we will discuss in this  
8 section so that they are directly applicable to our analyses of VGP dispersion in the CNS  
9 and the Jurassic.

10

11 This study will employ two sets of data. Group 1 includes only our ‘high quality’ data  
12 with  $n \geq 5$  and  $k \geq 50$ . Figure 3a and b show that, when  $N = 1000$ , the application of the  
13 within-site error correction to such data produces an estimate for  $S_B$  that is within  $1^\circ$  of  
14 the true value. Consequently, we expect Group 1 datasets to introduce no bias through  
15 low  $n$  and/or  $k$  effects (low  $N$  effects will be discussed shortly).

16

17 Group 2 will be used to verify observations made from the Group 1 datasets. It will have  
18 the advantage of including more data (increasing both  $N$  and the number of datasets  
19 available) but will include datasets with lower  $n$  and  $k$  values than those in group 1. Most  
20 significantly, some of these datasets will be from sites with  $n = 1$ . For  $n < 5$ , the  $k$  value  
21 becomes an unreliable measure of  $\kappa$  and for  $n = 1$ , there can be no estimate at all of how  
22 precise the measurement is. Nonetheless, this data can still be useful if it is dealt with  
23 carefully. If we chose to apply no within-site scatter correction to these results, then we

1 could expect to introduce some significant artefacts to our results, especially if the real  $S_B$   
2 is low. Figure 3c and 3d illustrates this and also shows the effects of ‘guessing’ the  $\kappa$   
3 value for datasets with  $n = 1$ . If one guesses it correctly, the  $S_W$  correction is reasonably  
4 effective and so long as the  $\kappa$  value is not underestimated, the situation is improved over  
5 that of not applying any  $S_W$  correction (shown by the  $k_{est} = \infty$  curve). If the within-site  
6 scatter of the directions is assumed to be higher than it actually is (i.e. if  $k$  is assumed to  
7 be much lower than  $\kappa$  actually is), then the  $S_W$  correction can severely bias the measured  
8 value of  $S_B$  to low values (shown by the  $k_{est} = 50$  curve).

9

10 The plots shown in figure 3c and d have significant implications for PSV studies which  
11 generate estimates for  $S_B$  using data from sedimentary rocks e.g. (Cronin et al., 2001;  
12 Kruiver et al., 2000). Since such studies are generally based on measurements of only 1  
13 sample per stratigraphic level, no estimate of  $S_W$  (the amount of random errors associated  
14 with the measurement process) is available and therefore no correction is made for this.  
15 This is equivalent to taking the  $k = \infty$  curve in figure 3c and d which, as shown, can lead  
16 to  $S_B$  being significantly overestimated particularly if its true value is low. Future studies  
17 of this type should apply some ‘within-site’ dispersion correction to help reduce this  
18 problem. Even if this dispersion is entirely unknown (i.e. if there is only one sample per  
19 stratigraphic level), an arbitrarily large assumed value of  $k$  (e.g. 600), will at least  
20 represent some improvement over the current assumed  $k$  value of infinity.

21

22 We wished to test the effects of applying a fixed  $S_W$  correction based on  $k = 182$  to all of  
23 the data used in this study with  $n < 5$ . The distribution of  $k$  values observed in those site

1 mean directions used in this study with  $n \geq 5$  can be very well-approximated with a log-  
2 normal distribution (figure 4a). We generated 10,000 synthetic values at random from  
3 such a distribution (figure 4b) and used these as  $\kappa$  values for the same number of  
4 synthetic mean directions from ten different palaeolatitudes. Figure 4c and d shows the  
5 VGP dispersion curves we would expect to observe given  $S_B = 5$  and  $S_B = 15^\circ$  if we  
6 applied a  $S_W$  correction (assuming a  $\kappa$  value of 182 for all sites) and if we did not. This  $S_W$   
7 correction acts to bring the dispersion curve much closer to the expected value in both  
8 cases. Consequently, based on the reasonable assumption that the distribution of  $\kappa$  values  
9 in our sites with  $n < 5$  is similar to that in our sites with  $n \geq 5$ , the application of a fixed  
10  $S_W$  correction based on  $k = 182$  in all sites should work reasonably well. We therefore  
11 apply this correction to our Group 2 data with  $n < 5$ .

12

### 13 *3.2 The effects of $N$ on measured VGP dispersion*

14 The largest constraint on effective measurement of VGP dispersion curves through  
15 geological time is the number of reliable site mean data available for them. This is  
16 especially the case for the present study because, unlike McFadden et al.(1991) who used  
17 plate tectonic reconstructions, we rely on the palaeomagnetic data itself (specifically the  
18 mean inclination) to define the palaeolatitude of each dataset.

19

20 We investigated the effects of different values of  $N$  (the number of site means per dataset)  
21 on a simulated analysis of PSV by drawing 10 synthetic datasets of  $N$  site mean directions  
22 for each latitude (figure 5). As one would expect, the range of values measured for the  
23 palaeolatitude and  $S_B$  is much larger when  $N$  is smaller. When the true value of  $S_B$  is  $15^\circ$

1 and  $N = 5$ , the inaccuracies introduced into measurements of both  $S_B$  and palaeolatitude  
2 are so large as to make the results of any single measurement essentially useless.  
3 Furthermore, the uncertainty limits produced for these estimates are also not reliable for  
4  $N < 18$  (see values of  $\Delta 95$  on figure 5).

5

6 As we might expect the amplitude of the noise produced by the low  $N$  effects is  
7 proportional to the actual (geomagnetic) value of  $S_B$ . This is demonstrated in the final  
8 panel of figure 5 where a simulated dispersion of  $S_B = 5^\circ$  with  $N = 5$  is shown for  
9 comparison with the other plots which have  $S_B = 15^\circ$ .

10

11 In this study, the paucity of data (particularly those that meet Group 1 criteria in the  
12 Jurassic period) is such that we were required to retain datasets with  $N < 18$  and even to  
13 use a few datasets with  $N < 10$ . In the latter case, we do not consider their estimates of  $S_B$ ,  
14 in themselves, to be reliable and therefore we employ them only in an indicative sense.

15

#### 16 **4. Sources of data**

##### 17 *4.1 Data from Lower Cretaceous lavas of the Gobi Altai*

18 This study was initiated as a consequence of a large dataset of site mean directions from  
19 Mongolian lavas from the Gobi Altai region for the CNS becoming available (Hankard et  
20 al, 2005; 2007; van Hinsbergen et al, 2008). In this paper, we present new data from 68  
21 lavas from the Gobi Altai (Table A1), which were specifically sampled for a PSV study.  
22 Fourteen lavas were sampled with two samples each in section Jaran Bogd, in addition to  
23 16 lava sites with  $n = 7$ , already reported earlier in van Hinsbergen et al. (2008).

1 Moreover, 54 consecutive lavas were sampled with one sample each in a ~1 km thick  
2 volcanic stratigraphy in section Kharaat Uul, southeast of Mt. Arz Bogd. For exact  
3 locations, age details, demagnetisation procedures and rock magnetic properties we refer  
4 to van Hinsbergen et al. (2008). The directions used here are corrected for bedding tilt,  
5 which amounts 5-10°. Table 1 and figure 6 summarises the Gobi Altai lava data for the  
6 CNS; all directions that were not clearly lightning-induced remagnetisations are  
7 included.

8

9 The data are split into two groups based on the mean inclination of the directions. Sites  
10 from the Southeast Artz Bogd region (which we will term the SEAB group) display  
11 clearly steeper inclinations (~8°) than those from the rest (which we term non-SEAB).  
12 This is extremely unlikely to reflect a difference in palaeolatitude (of ~10°) between the  
13 two groups. The Gobi Altai lavas (apart from the SEAB) display indistinguishable mean  
14 directions from one another which strongly suggests that the region was at polar standstill  
15 for the period during which they were emplaced (95-125 Ma; Hankard et al, 2007; van  
16 Hinsbergen et al, 2008). Van Hinsbergen et al. (2008) presented two possible  
17 explanations for the discrepancy of the SEAB directions. The first is that the directions do  
18 not adequately sample the variation of the geomagnetic field and therefore over-represent  
19 a particular spell of PSV. The second is that these particular lavas were not emplaced  
20 horizontally and that, in making a bedding plane correction to the measured directions of  
21 remanence, an artificially steep inclination was introduced.

22

1 Several observations made in this study make it appear that the second explanation given  
2 above is the more likely. The full SEAB dataset has a larger VGP dispersion than that of  
3 the non-SEAB dataset (tables 1 and 3). Furthermore, there is strong evidence for serial  
4 correlation of directions in only a small proportion of the SEAB lavas (the 7 lavas of the  
5 Kharaat Uul which were sampled with more than one core are the only ones with NRO  
6 factor  $> 0.95$ ; table 1). Consequently, we retain the SEAB data for the PSV analysis  
7 (section 5), but modify its palaeolatitude so that it is equal to that of the non-SEAB  
8 dataset.

9

10 In the non-SEAB dataset, the NRO factor is highly significant for several localities (table  
11 1) including two of those (Jaran Bogd and Bulgantiin Uul) where sedimentary layers  
12 were found between individual lavas. This is similar to the observation made by Knight et  
13 al. (2004) for Moroccan lavas from the Central Atlantic Magmatic Province (CAMP) and  
14 suggests very rapid deposition of the sedimentary horizons. However, the mean directions  
15 from the majority of non-SEAB localities are highly consistent (figure 6a) despite them  
16 being erupted in pulses of volcanism (see van Hinsbergen et al., 2008 for more details)  
17 which together spanned a period of more than 30 Myr. This strongly suggests that data  
18 from most of the localities largely average the PSV regardless of whether they exhibit  
19 serial correlation. One locality (Khalzan Khairkhan) has a mean direction slightly away  
20 from the rest as well as NRO factor of 0.99; these data likely do not average PSV on their  
21 own but may be combined with the rest.

22

23 *4.2 Data from the literature*

1 We searched the global palaeomagnetic database (GPMDB;  
2 <http://www.ngu.no/dragon/Palmag/paleomag.htm>) and the recent literature for suitable  
3 data for analysing PSV in the CNS and in the Jurassic period. Our criteria were:

4

- 5 1. Data from lavas and welded tuffs, with an age range entirely within the CNS (84-  
6 125 Ma) or the Jurassic (145-200 Ma). A few data from non-welded tuffs and  
7 dykes were also included (tables 2 and 3) - the reliability of the estimates of  $S_B$   
8 which are derived from these will be discussed in the next section.
- 9 2. Every manuscript was checked and the data were excluded if there were any  
10 suspicion of the directions not being primary or affected by uncertain post-  
11 emplacement tilting.
- 12 3. The samples must have undergone stepwise demagnetisation to isolate the  
13 characteristic remanence. This corresponds to the directions have a ‘demag code’  
14 in the GPMDB of 3 or higher.
- 15 4. The dataset must comprise site mean directions from at least 7 individual rock  
16 units (i.e.  $N \geq 7$ ).

17

18 Datasets which passed the four criteria above are termed Group 2 here. The subset of  
19 these which also have individual site mean data with  $n \geq 5$  and  $k \geq 50$  have both a  
20 reasonable within-site scatter (although the definition of ‘reasonable’ is of course  
21 arbitrary) and a good number of samples with which to estimate this characteristic; they  
22 are termed Group 1.

23

1 The Group 1 and Group 2 data from both time periods are summarised in tables 2 and 3.  
2 Two NRO factors are given. *NRO factor 1* is that obtained when all the data in the set are  
3 input together grouped by the localities where they were obtained; it therefore is a  
4 measure of the amount of clustering of the data by locality rather than progressive serial  
5 correlation. *NRO factor 2* is that measured from data obtained from a stratigraphic  
6 sequence of units and therefore may reflect a gradual progression in directions. When a  
7 dataset contained more than one stratigraphic sequence, the lowest *NRO factor 2*  
8 measured is given.

9

10 These NRO factors are frequently significant (i.e.  $> 0.95$ ) indicating that, in a great many  
11 cases, bursts of extrusive activity caused series of lavas to record related periods of  
12 geomagnetic behaviour. However, most of the datasets have *either* the first or the second  
13 NRO factor less than 0.95 and this is all that is required for the dataset to provide what is  
14 likely a reasonable representation of field variations. If *NRO factor 1* is low then it  
15 indicates that directions taken from different localities are not clustered suggesting that  
16 each group contains approximately the full range of geomagnetic behaviour. If *NRO*  
17 *factor 2* is low, it indicates that at least one sampled stratigraphic section contains data  
18 that likely represents a statistically random sampling of the field.

19

20 On this basis, two Group 1 datasets present a significant risk of giving an estimate of  $S_B$   
21 which is biased to low values - the Rajmahal Traps and Balantak. Two of the larger  
22 datasets: Lesotho and the CAMP are, together with the new Gobi Altai data (discussed in  
23 section 4.1), clearly heavily affected by short duration bursts of volcanic activity resulting

1 in the measurements being placed into ‘directional groups’ in the original studies (Knight  
2 et al., 2004; Kostrov and Perrin, 1996). However, in both of these cases, we suspect that  
3 the volume of data allows us to have a largely unbiased estimate of  $S_B$ .

4

5 While the Lesotho dataset produces NRO factors 1 and 2 of 0.99, the directions from  
6 these basalts pass a reversal test which suggests adequate representation of the SV; its  
7 mean pole is also within errors of other Jurassic poles for South Africa further supporting  
8 this (Kostrov and Perrin, 1996). Knight et al. (2004) split their data from the Central  
9 Atlantic Magmatic Province (CAMP) basalts in Morocco into 7 directional groups, each  
10 representing a distinct spell of secular variation, which they numbered DG1 to DG7.  
11 They excluded DG4 for having reversely magnetised lavas and DG7 because it was from  
12 a unit of uncertain age and demonstrated that the overall mean direction produced by the  
13 other DG means (Dec = 344°, Inc = 41°, N = 5, k = 24.3) gave a pole indistinguishable  
14 from that of the mean pole for Africa at 200 Ma. Here we use as our dataset the  
15 combination of all the data from these same 5 directional groups. These produce a mean  
16 (Dec = 349°, Inc = 42°, N = 62, k = 21.2) which is very similar in direction and dispersion  
17 to the DG mean and which therefore is unlikely to be biased by over-representation of  
18 any particular period(s) of secular variation.

19

20 Welded tuffs were clearly emplaced above the Curie temperature of the ferromagnetic  
21 minerals they contain and therefore carry a spot-reading of the field most likely as a  
22 thermoremanent magnetisation (TRM). Other tuff and ignimbrite units were potentially  
23 emplaced at lower temperatures which could cause them to retain a Depositional

1 Remanent Magnetisation (DRM) instead. If this was the case, and if layers of the  
2 pyroclastic deposits accumulated over centuries, then there is the potential for datasets  
3 containing tuffs to underestimate  $S_B$  because of averaging effects. This potential biasing  
4 effect will be discussed on a point by point basis in the next section.

5

6 Only two datasets - Vestfjella and Lembobo - have a significant proportion of their  
7 measurements produced from intrusive rocks. In both cases, the thicknesses of the  
8 sampled units are not given. However, their stated composition (basaltic and rhyolitic  
9 respectively) is suggestive of them cooling rapidly which implies that they are unlikely to  
10 bias the estimate of  $S_B$  significantly through slow-cooling.

11

## 12 **5. Results**

### 13 *5.1 Group 1 datasets*

14 Figure 7a and b summarise the results produced from group 1 datasets for both periods. It  
15 shows that the choice of whether to use a fixed 45° cutoff or the variable cutoff  
16 developed by Vandamme (1994) makes little or no difference to the VGP dispersion  
17 curve produced in both periods.

18

19 The datasets are far too small and few to make any meaningful test for equatorial  
20 asymmetry in the VGP dispersion recorded in both periods. However, given that figure 7a  
21 and b show no obvious evidence of asymmetry and that the geocentric axial dipole  
22 (GAD) hypothesis is normally assumed to be reasonable for these periods, we choose to

1 plot the data from the N and S hemisphere on the same axis in figure 7c and d and to  
2 apply the variable VGP cutoff.

3

4 The CNS datasets appear to show rather consistent  $S_B$ - $\lambda$  behaviour (figure 7c). In  
5 particular, at mid-latitudes we have datasets from five geographically distinct areas (three  
6 in the N and two in the S hemisphere) giving  $S_B$  values within errors of one another. One  
7 of these, the Spences Bridge dataset (with  $\lambda = 48.7$ ) is marked with an asterisk in tables 2  
8 and 3 because Irving and Thorkelson (1990) noted that there was the potential for (small)  
9 errors in the correction to the palaeohorizontality. However, the good agreement of this  
10 dataset's estimate of  $S_B$  with the other four from similar palaeolatitudes suggests that this  
11 was not too serious a problem. The Balantak dataset (with  $\lambda = -19.7$ ) has some doubts  
12 associated with its Cretaceous age (Kadarusman et al., 2004) and may instead be Tertiary.  
13 While we cannot comment on this uncertainty, we do note here that it fits the overall  
14 trend of the CNS data excellently. Similarly, the consistency displayed by the Mongolia  
15 SEAB dataset with others from a similar inferred palaeolatitude provides some support  
16 for our decision to manually adjust its value of  $\lambda$  (section 4.1). Since the three datasets  
17 mentioned above do not strongly influence the fit of the Model G curve to the Group 1  
18 data, their exclusion would only serve to unnecessarily reduce our confidence in this fit;  
19 they are therefore all retained.

20

21 The Jurassic datasets comprise little over half as much data as those in the CNS and are  
22 limited to a very short low to mid-latitudinal range in both hemispheres (figure 7d). The  
23 lowest  $S_B$  value displayed in figure 7b and d is from the Manzhouli dataset which

1 comprises data taken from tuffs which gave an inconclusive result when subjected by us  
2 to the reversal test. This may indicate that the full range of SV is not represented in this  
3 dataset and that  $S_B$  is underestimated as a result. Because of this doubt and because of the  
4 strong influence it would exert, we exclude this dataset from the Model G curve fit.

5

6 Given the limitations to the Jurassic data described above, it is not possible to compare  
7 the VGP dispersion curves in figure 7c and 7d with any real confidence. There is a  
8 suggestion that mean  $S_B$  is lower for the low latitude sites in the CNS than in the Jurassic  
9 and that mean  $S_B$  is more dependent on palaeolatitude in the CNS. These are qualitatively  
10 the same observations as made by McFadden et al. (1991) when comparing VGP  
11 dispersion curves for their periods 80-110 Ma and 110-195 Ma. In terms of the Model G  
12 of McFadden et al. (1988), this corresponds to the CNS data producing a lower  $a$  value  
13 and a higher  $b$  value than the Jurassic data. A more convincing observation to be made  
14 from figure 7 is that the values of  $S_B$  have a much less predictable relationship with  
15 palaeolatitude in the Jurassic than in the CNS. This may be only partly explained by the  
16 lower values of  $N$  for the Jurassic datasets which will tend to increase the scatter (figure  
17 5) of measured  $S_B$  values.

18

19 We will now turn to the larger, lower quality datasets in Group 2 to see if these can verify  
20 the observations made above to any degree.

21

22 *5.2 Group 2 datasets*

1 While the choice of fixed or variable cutoff makes little difference to the CNS datasets,  
2 several of the Jurassic datasets give significantly lower values of  $S_B$  with the latter  
3 employed. Since lower quality data (in particular those with  $n = 1$ ) are more likely to be  
4 unreliable outliers, we choose to apply the variable cutoff prescribed by Vandamme  
5 (1994) to the data in figure 8c and d since this is likely to be more effective at excluding  
6 them.

7

8 Figure 8c shows that the Group 2 datasets from the CNS produce a similar VGP  
9 dispersion plot to their Group 1 equivalents and therefore verify the strong latitudinal  
10 dependence of  $S_B$ . Two Group 2 datasets (Vinita and Mt. Somers) comprise a significant  
11 number of directions from tuff units. However, both these datasets give consistent  $S_B$   
12 values to those of others from similar palaeolatitudes and therefore do not appear to be  
13 strongly biased by time-averaging effects. Model G fitted to the Group 2 datasets has a  
14 slightly higher (though well within error)  $a$  parameter than that fitted to the Group 1  
15 datasets which may indicate that the values of  $S_B$  in the former are marginally increased  
16 by the inclusion of poorer quality data (c.f. figure 4c and d).

17

18 The situation for the Jurassic Group 2 datasets is not so clear cut. They, like their Group 1  
19 equivalents, are also rather scattered but now some mean latitudinal dependence, similar  
20 to that for the CNS data, is implied in figure 8d.

21

22 This newly observed relationship is not a consequence of the inclusion of non-lava data  
23 which average out PSV. While the Jurassic Lepa dataset is dominated by directions from

1 tuffs, it has a higher than average  $S_B$ . The Zymoetz dataset which contains data from both  
2 lavas and tuffs in unknown proportion also does not give an unusually low  $S_B$  value.  
3 Nonetheless, given the large variation in  $S_B$  values measured for the Jurassic coupled with  
4 the small palaeolatitudinal span of the datasets, we cannot rule out the apparent latitudinal  
5 dependence of mean  $S_B$  being an artefact of a few inaccurate datasets having a  
6 disproportionate weight. For example, the two datasets with the highest palaeolatitudes  
7 (North El Quemado and Marifil) are both taken from the same study and are crucial in  
8 defining the non-zero slope of the mean  $S_B$ - $\lambda$  relationship.

9

10 We also note that the application of the fixed cutoff to the Group 2 Jurassic datasets  
11 produces a mean latitudinal dependence of  $S_B$  that is weaker even than that observed in  
12 figure 8d. A simple linear regression analysis through the VGP dispersion plots of either  
13 the variable ( $R^2 = 0.086$ ) or the fixed ( $R^2 = 0.043$ ) cutoff data is not significant at the 90%  
14 confidence level. Consequently, the suggested relationship in figure 8d is not robust.

15

16 Our analysis of Group 2 Jurassic data is inconclusive but fails to verify the comparisons  
17 of *mean* VGP dispersion behaviour made in section 5.1 (i.e. that  $a$  is lower and  $b$  higher  
18 in the CNS than in the Jurassic). It does, however, offer some support for the observation  
19 that  $S_B$  is much more predictable for CNS datasets than it is for Jurassic ones which itself  
20 is an interesting difference and will be discussed.

21

22 **6. Discussion**

1 We have performed a detailed analysis of PSV in the CNS and Jurassic using an updated  
2 database and with careful checking for potential sources of bias. The Group 1 and Group  
3 2 datasets are complementary and provide a means for verifying the observations made  
4 from one another. The former datasets are most likely free from biasing effects due to  
5 palaeomagnetic measurement errors but are at increased risk of being inaccurate due to  
6 having low values of  $N$ . The Group 2 datasets, by contrast, are lower quality but both  
7 larger and more numerous. The agreement between figure 7c and 8c indicates that we can  
8 have some confidence in the relationship of the mean VGP dispersion with palaeolatitude  
9 shown for the CNS time period. Group 1 and Group 2 datasets produce similar and  
10 similarly well-defined VGP dispersion curves indicating that this relationship is unlikely  
11 to be an artefact of either small  $N$  or small  $n$ . After examining each dataset closely, we  
12 conclude that it is also unlikely to be due to inadequate sampling of PSV (or its time  
13 averaging) by any particular datasets.

14

15 We would like to compare the pattern of mean VGP dispersion in the CNS to that in the  
16 Jurassic but this is not possible as it is not clear what the pattern in the earlier period was.  
17 The Group 1 data show a flat mean VGP dispersion curve (figure 7d) but this could be a  
18 product of the small values of  $N$  introducing noise; the Group 2 datasets produce an  $S_B$ - $\lambda$   
19 curve which is more similar to those of the CNS datasets but this may be due to the  
20 disproportionate influence of a few low-quality data. The uncertainty is further  
21 compounded by the severely limited palaeolatitudinal range of the Jurassic datasets.

22

1 Fortunately, we are not reliant on Jurassic datasets to provide a first test that average  
2 reversal frequency and PSV are related. The results of a recent analysis performed by  
3 Johnson et al. (2008) of datasets from the period 0-5 Ma (when average reversal  
4 frequency was  $4.0 \text{ Myr}^{-1}$ ) are shown in figure 9. This analysis featured directional data  
5 with  $n \geq 5$  and  $k \geq 50$  in some cases and  $n \geq 5$  and  $k \geq 100$  in others. Consequently, their  
6 data was of at least the same reliability as the Group 1 data used in this study and far  
7 more numerous (although they also suffered from a paucity of data at high latitudes).

8

9 Figure 10 compares VGP dispersion curves of binned datasets from Group 1 and 2 data  
10 for both the CNS and the Jurassic with the binned Johnson et al. data. The 0-5 Ma data  
11 was treated using a fixed  $45^\circ$  cutoff rather than a variable cutoff so, for the purpose of  
12 this comparison, we treated the CNS and Jurassic data in the same way before binning  
13 them. This comparison reveals that both Group 1 and Group 2 CNS curves are below the  
14 0-5 Ma curve at low palaeolatitudes and that the overall relationship with palaeolatitude  
15 is stronger (gradient more positive) in the CNS curves. As expected, the binned Group 1  
16 Jurassic VGP dispersion curve is similar to the 0-5 Ma curve for the palaeolatitude range  
17 where there are data whereas the Group 2 Jurassic curve is more variable.

18

19 There is a potential source of bias that may have increased the estimates of  $S_B$  made in  
20 this study but which will not have affected the analysis of Johnson et al. (2008). This is  
21 the effect of errors made in the measurement of the palaeohorizontal at sampled sites. The  
22 extent of this error is extremely uncertain but is unlikely to exceed  $\pm 5^\circ$  in both the strike  
23 and dip measured in most cases. This maximum error may be approximated by a Fisher

1 distributed scatter function (in direction-space) with  $k \approx 400$  which translates in pole-  
2 space to an enhanced  $S_B$  of  $\sim 1^\circ$  at low latitudes and  $\sim 2^\circ$  at higher latitudes. The  
3 implications of taking this source of bias into account for figure 10 is to slightly  
4 strengthen our conclusion that  $S_B$  is lower at low palaeolatitudes in the CNS datasets  
5 relative to the 0-5 Ma datasets and to slightly weaken our conclusion that the values of  $S_B$   
6 in the CNS are more dependent on palaeolatitude.

7

8 Another potential source of noise for the measured values of  $S_B$  this study lies in the  
9 possibility that the original dip of volcanic units was mistaken for tectonic dip (and  
10 therefore corrected for unnecessarily). As discussed earlier (section 4.1), this was  
11 considered to be a problem for the Mongolia SEAB dataset which we overcame by  
12 manually adjusting its inferred palaeolatitude. In general however, we would expect this  
13 to be more of a problem in intermediate to felsic units (andesites, rhyolites, ignimbrites,  
14 and tuffs) than in basalts because the higher viscosity of the former tends to produce  
15 steeper gradients. The Group 1 CNS datasets consist mostly of basalts and produces a  
16 coherent  $S_B$ - $\lambda$  curve (figure 7c). Similar, coherent behaviour is also exhibited by the  
17 group 2 datasets which consist of other materials. There is therefore a reasonable case to  
18 be made that the CNS datasets are unlikely to be significantly affected by this lithological  
19 problem. Unfortunately, since numerous datasets from both Group 1 and 2 comprise data  
20 from intermediate to felsic material and since these do not display coherent behaviour in  
21 figures 7d and 8d, we cannot rule out that they are affected by this problem.

22

1 The Jurassic Group 1 and Group 2 datasets do display a similarly high degree of scatter  
2 between their  $S_B$  datasets and we argue that this is probably not entirely due to introduced  
3 noise. For example, the CAMP and Lesotho datasets both comprise a large number of  
4 directions from basaltic flows which were inferred to have erupted at mid to low  
5 palaeolatitudes within  $\sim 20$  Myr of one another. Yet their calculated values of  $S_B$  differ by  
6  $6-8^\circ$  (40-60 %; tables 2 and 3). We therefore argue that the value of  $S_B$  is inherently less  
7 certain (i.e. more variable) in the Jurassic than in the CNS.

8

9 This same argument may also apply to a comparison of the 0-5 Ma and the CNS periods.  
10 Given that the average value of  $N$  for the 0-5 Ma datasets is much larger than that for the  
11 CNS datasets, we would expect the 0-5 Ma VGP dispersion curve to be much more  
12 coherent than the CNS curves (c.f. figure 5). However, figure 9 indicates that this is  
13 certainly not the case which suggests that the variation of  $S_B$  with palaeolatitude may be  
14 more constant in the CNS than in the last 5 Myr also.

15

16 It therefore appears that in the CNS, the pattern of PSV was much more consistent  
17 through time than it was through the Jurassic period or even the last 5 Myr. This could be  
18 explained by periods of higher reversal frequency having a greater rate of change of PSV  
19 in time. This hypothesis appears to be supported by a study of the historical field (Hulot  
20 and Gallet, 1996) which showed that “instantaneous” VGP dispersion curves (where each  
21 dispersion value represents the longitudinal variation in the field along a line of latitude)  
22 obtained from the 1980, 1900, and 1800 fields were significantly different (see also figure  
23 1b). It is also consistent with the range of instantaneous VGP curves being much reduced

1 for the Glatzmaier-Roberts Model E than for their Model G (compare the standard  
2 deviations shown by the error bars for the two VGP dispersion curves shown in figure 1).

3

4 The findings of this study, regarding the shapes of VGP dispersion curves from periods  
5 with different mean reversal frequencies, are (for Group 1 data at least) qualitatively  
6 similar to those reported by McFadden et al. (1991) but far more equivocal. Figure 11  
7 shows that there may well be a relationship between the shape of the mean VGP  
8 dispersion curve and average reversal frequency but that it is implied to be much more  
9 subtle than that reported by the previous study. Our fit of Model G to the CNS data given  
10 in McFadden et al. (1991, their table 6) has parameters  $a = 6.1$  and  $b = 0.34$  while that fit  
11 to their 110-195 Ma data (their table 7) gave  $a = 18.2$  and  $b = 0.14$ . The differences in  
12 these parameters (particularly  $a$ ) measured for the two periods was much larger for their  
13 data than for ours and it is worthwhile discussing potential reasons for this.

14

15 Firstly, we point out that the far larger and higher quality set of data used in the present  
16 study implies that its findings should be much more trustworthy. To clarify: less than  
17 25% of the data used in this study were published at the time McFadden et al's database  
18 was compiled (1983) and it is possible that as much as 35% of their data did not pass our  
19 Group 1 or Group 2 criteria (they used the period 110-195 Ma instead of the Jurassic  
20 which prevents a direct comparison). Furthermore, we used more than two and a half  
21 times as much data in our study as they did in their combined period 80-195 Ma. We  
22 would expect these differences to cause the results of the present study to be less noisy  
23 and therefore less equivocal than those obtained by McFadden et al. (1991).

1

2 The fact that the opposite is true is likely to be at least partially due to McFadden et al.  
3 (1991) applying a constant  $S_W$  correction to all their data for which they did not have  
4 sufficient information to estimate it (we could not obtain their database and therefore do  
5 not know the proportion of data this entails but we expect that it was significant). For this  
6 correction, they took the median  $S_W$  value of their other lavas which was  $14^\circ$  (translating  
7 to a median  $k$  value of approximately 60 - as an aside, it is worth noting that this is much  
8 lower than our median  $k$  value of 182 which indicates the lower quality of their datasets).  
9 However, since  $S_W$  is defined in pole-space, this translates to unrealistic latitudinally-  
10 dependent dispersion in direction-space ( $k$  ranging from 12 for sites at the equator to 134  
11 for sites at the poles). Note the difference between their approach and that employed by  
12 this study: we used the  $k$  value to define within-site dispersion because random errors  
13 associated with the measurement process will affect directions similarly regardless of site  
14 latitude. The consequence for their analysis is that their within-site scatter correction will  
15 have been overly large for sites with low palaeolatitude and insufficiently large for sites  
16 with high palaeolatitude.

17

18 Figure 12 shows the effect of using McFadden et al's approach to analyse simulated  
19 datasets with different values of (latitudinally-constant)  $S_B$ . A latitudinally-dependent  
20 artefact is introduced which becomes more exaggerated the smaller that the real  $S_B$  is.  
21 The effect of this artefact would be to amplify any small genuine differences in  $S_B$ . This  
22 is likely to be the main reason why McFadden et al. (1991) observed a much more clear-  
23 cut relationship between PSV and reversal frequency than we do. It may well also explain

1 why they observed a strong anticorrelation between the  $a$  and  $b$  parameters of the Model  
2 G fit to their different time windows.

3

4 Although the relationship between average reversal frequency and PSV as described by  
5 VGP dispersion curves is apparently less obvious than that reported by McFadden et al.  
6 (1991), a relationship does appear to exist (figure 11) and it is qualitatively very similar  
7 to that claimed previously. This is the same conclusion Tarduno et al. (Tarduno et al.,  
8 2002) made with a smaller dataset and is important because it shows that the PSVL  
9 technique may be used, alongside or instead of magnetostratigraphy, to determine the  
10 first order stability of the geodynamo at other times in the Earth's history. It has already  
11 been used for this purpose in studying the late Archaean-early Proterozoic geodynamo  
12 (Biggin et al., 2008; Smirnov and Tarduno, 2004) and the findings of the present study  
13 strengthen the conclusions obtained. The shape of the VGP dispersion curve produced by  
14 Biggin et al. (2008) implies that the geodynamo was more stable in the late Archaean -  
15 early Proterozoic than most likely at any time in the last 200 Myr. Furthermore, the high  
16 degree of consistency observed in the  $S_B$  values produced from datasets with similar  
17 palaeolatitudes implies a low rate of change of PSV pattern which is also consistent with  
18 increased dynamo stability as observed in this study.

19

20 VGP dispersion curves remain the most common and obvious means of analysing PSVL  
21 data. However, the shape of a curve is influenced by non-unique factors (Hulot and  
22 Gallet, 1996) and is not easy to interpret in physical terms. McFadden et al. (1988)  
23 showed that the equatorially antisymmetric spherical harmonic components of the 1980

1 IGRF field model produced an instantaneous VGP dispersion curve that was zero at the  
2 equator and strongly latitudinally dependent. Conversely, the equatorially symmetric  
3 components produced a VGP dispersion curve that was more or less constant (and  
4 nonzero) with latitude.

5

6 Hulot & Gallet (1996) confirmed this observation for the 1900 and 1800 field models but  
7 also showed that almost all of the VGP dispersions evident in both families was produced  
8 by variations in just four components: (1,1), (2,1), (3,1), and (4,1). If the same is assumed  
9 to apply to the dynamo hundreds of millions of years ago then this might imply that  
10 variations in the equatorial dipole (1,1) and equatorial octupole (3,1) components were  
11 suppressed during the CNS relative to the last 5 Myr (and possibly the Jurassic as well).  
12 This is consistent with the conclusion reached by Tarduno et al. (2002), made using a  
13 completely different type of analysis (a transect of inclination versus expected colatitude  
14 made along the North American craton), that the axial octupole was suppressed during  
15 the CNS.

16

## 17 **7. Conclusions**

18 1. Directional data with low  $n$  (from either igneous or sedimentary rocks) may be  
19 used to study PSV but such data should be treated cautiously (e.g. in this study,  
20 we use Group 2 data only to verify the conclusions produced from higher quality  
21 Group 1 data). When low  $n$  (even  $n = 1$ ) data is used, a within-site error correction  
22 should be estimated and applied. However, this estimate should err to low values  
23 to avoid over-correction which can significantly bias VGP dispersion curves.

1

2 2. The clear-cut relationship between PSV and mean reversal frequency observed by  
3 McFadden et al. (1991) for the last 195 Myr was very likely, at least in part, an  
4 artefact introduced by their analytical procedure. We expect that their application  
5 of a constant within-site scatter correction in pole-space will have tended to  
6 exaggerate small differences in their VGP dispersion curves caused by  
7 geomagnetic variations.

8

9 3. The above conclusion notwithstanding, subtle differences in VGP dispersion  
10 curves, of a qualitatively similar nature to those reported by McFadden et al.  
11 (1991) and Tarduno et al. (2002), are evident between the data collated by this  
12 study from the CNS and that collated by Johnson et al. (2008) for 0-5 Ma. This  
13 suggests that SV and reversal frequency are linked and that PSVL may be used as  
14 a tool to determine first-order variability in geodynamo stability.

15

16 4. A number of problems associated with the Jurassic datasets preclude any certainty  
17 about the relationship of mean VGP dispersion with palaeolatitude for this period.  
18 These datasets were frequently small in size and associated with intermediate to  
19 felsic lithologies (and therefore may have had a significant original dip);  
20 furthermore, they spanned a very limited palaeolatitudinal range and the Group 1  
21 and Group 2 data did not produce similar  $S_B$ - $\lambda$  curves. More reliable data from  
22 igneous rocks of Jurassic age, and particularly those formed at higher  
23 palaeolatitudes, are badly needed.

1

2 5. The pattern of PSV, as measured by VGP dispersion with palaeolatitude, appears  
3 to have been less time-dependent in the CNS than in both the Jurassic (but see  
4 conclusion 4 above) and the 0-5 Ma periods. This is suggestive of a relationship  
5 also observed in the Glatzmaier-Roberts dynamo model (Glatzmaier et al., 1999)  
6 whereby the reversal frequency is higher during periods when ‘instantaneous’  
7 VGP dispersion curves are more variable in time.

8

### 9 **Acknowledgements**

10 This research was undertaken with funding provided by the Netherlands Science  
11 Foundation (NWO) and conducted under the programme of the Vening Meinesz  
12 Research School of Geodynamics (VMSG). Research by DJJvH was supported by  
13 UK/NERC grant NER/D/S/2003/00671 and an NWO-VENI grant. We are extremely  
14 grateful to Gary Glatzmaier for providing us with simulated data and to John Tarduno  
15 and an anonymous reviewer for comments which helped improve the manuscript.

16

### 17 **References**

- 18 Biggin, A.J., Strik, G. and Langereis, C.G., 2008. Evidence for a very long-term-trend in  
19 geomagnetic secular variation. *Nature Geoscience*, 1: 395-398.
- 20 Biggin, A.J. and Thomas, D.N., 2003. Analysis of long-term variations in the  
21 geomagnetic poloidal field intensity and evaluation of their relationship with  
22 global geodynamics. *Geophysical Journal International*, 152(2): 392-415.
- 23 Courtillot, V. and Olson, P., 2007. Mantle plumes link magnetic superchrons to  
24 Phanerozoic mass depletion events. *Earth and Planetary Science Letters*, 260:  
25 495-504.
- 26 Cox, A., 1970. Latitudinal dependence of the angular dispersion of the geomagnetic field.  
27 *Geophysical Journal of the Royal Astronomical Society*, 20: 253-269.
- 28 Cronin, M., Tauxe, L., Constable, C., Selkin, P. and Pick, T., 2001. Noise in the quiet  
29 zone. *Earth and Planetary Science Letters*, 190(1-2): 13-30.

- 1 Fisher, R.A., 1953. Dispersion on a sphere. *Proceedings of the Royal Society of London*,  
2 A217: 295-305.
- 3 Glatzmaier, G.A., Coe, R.S., Hongre, L. and Roberts, P.H., 1999. The role of the Earth's  
4 mantle in controlling the frequency of geomagnetic reversals. *Nature*, 401(6756):  
5 885-890.
- 6 Glatzmaier, G.A. and Roberts, P.H., 1995. A 3-Dimensional Self-Consistent Computer-  
7 Simulation of a Geomagnetic-Field Reversal. *Nature*, 377(6546): 203-209.
- 8 Gong, Z., Langereis, C.G. and Mullender, T.A.T., 2008. The rotation of Iberia during the  
9 Aptian and the opening of the Bay of Biscay. *Earth and Planetary Science Letters*,  
10 In Press.
- 11 Gradstein, F.M., Ogg, J.G. and Smith, A.G. (Editors), 2004. *A Geologic Time Scale*  
12 2004. Cambridge University Press, Cambridge, 589 pp.
- 13 Gregor, C.B., Mertzman, S., Nairn, A.E.M. and Negendank, J., 1974. The  
14 paleomagnetism of some Mesozoic and Cenozoic volcanic rocks from the  
15 Lebanon. *Tectonophysics*, 21: 375-395.
- 16 Gubbins, D., 1994. Geomagnetic Polarity Reversals - a Connection with Secular  
17 Variation and Core-Mantle Interaction. *Reviews of Geophysics*, 32(1): 61-83.
- 18 Gubbins, D., 1999. The distinction between geomagnetic excursions and reversals.  
19 *Geophysical Journal International*, 137(1): F1-F3.
- 20 Hankard, F., Cogne, J.P. and Kravchinsky, V., 2005. A new Late Cretaceous  
21 paleomagnetic pole for the west of Amuria block (Khunnen Uul, Mongolia). *Earth*  
22 *and Planetary Science Letters*, 236(1-2): 359-373.
- 23 Hankard, F., Cogne, J.P., Quidelleur, X., Bayasgalan, A. and Lkhagvadorj, P., 2007.  
24 Palaeomagnetism and K–Ar dating of Cretaceous basalts from Mongolia.  
25 *Geophysical Journal International*, 169: 898–908.
- 26 Henthorn, D.I., 1981. The magnetostratigraphy of the Lebombo Group along the Olifants  
27 River, Kruger National Park. *Annals of the Geological Survey of South Africa*,  
28 15: 1-10.
- 29 Hulot, G. and Gallet, Y., 1996. On the interpretation of virtual geomagnetic pole (VGP)  
30 scatter curves. *Physics of the Earth and Planetary Interiors*, 95(1-2): 37-53.
- 31 Iglesia Llanos, M.P.I. et al., 2003. Palaeomagnetic study of the El Quemado complex and  
32 Marifil formation, Patagonian Jurassic igneous province, Argentina. *Geophysical*  
33 *Journal International*, 154(3): 599-617.
- 34 Irving, E. and Thorkelson, D.J., 1990. On Determining Paleohorizontal and Latitudinal  
35 Shifts - Paleomagnetism of Spences Bridge Group, British-Columbia. *Journal of*  
36 *Geophysical Research-Solid Earth and Planets*, 95(B12): 19213-19234.
- 37 Jackson, A., Jonkers, A.R.T. and Walker, M.R., 2000. Four centuries of geomagnetic  
38 secular variation from historical records. *Philosophical Transactions of the Royal*  
39 *Society of London Series a-Mathematical Physical and Engineering Sciences*,  
40 358(1768): 957-990.
- 41 Johnson, C.L. et al., 2008. Recent Investigations of the 0–5 Ma Geomagnetic Field  
42 Recorded by Lava Flows. *Geochemistry Geophysics Geosystems*: doi:  
43 10.1029/2007GC001696, in press.
- 44 Kadarusman, A., Miyashita, S., Maruyama, S., Parkinson, C.D. and Ishikawa, A., 2004.  
45 Petrology, geochemistry and paleogeographic reconstruction of the East Sulawesi  
46 Ophiolite, Indonesia. *Tectonophysics*, 392(1-4): 55-83.

- 1 Klotwijk, C.T., 1971. Palaeomagnetism of the Upper Gondwana-Rajmahal Traps, NE  
2 India. *Tectonophysics*, 12: 449-467.
- 3 Kluth, C.F., Butler, R.F., Harding, L.E., Shafiqullah, M. and Damon, P.E., 1982.  
4 Paleomagnetism of late Jurassic rocks in the Northern Canelo Hills, Southeastern  
5 Arizona. *Journal of Geophysical Research*, 87: 7079-7086.
- 6 Knight, K.B. et al., 2004. The central Atlantic magmatic province at the Triassic-Jurassic  
7 boundary: paleomagnetic and Ar-40/Ar-39 evidence from Morocco for brief,  
8 episodic volcanism. *Earth and Planetary Science Letters*, 228(1-2): 143-160.
- 9 Kostrov, A.A. and Perrin, M., 1996. Paleomagnetism of the Lesotho basalt, southern  
10 Africa. *Earth and Planetary Science Letters*, 139(1-2): 63-78.
- 11 Kruiver, P.P., Dekkers, M.J. and Langereis, C.G., 2000. Secular variation in Permian red  
12 beds from Dome de Barrot, SE France. *Earth and Planetary Science Letters*,  
13 179(1): 205-217.
- 14 Larson, R.L. and Olson, P., 1991. Mantle Plumes Control Magnetic Reversal Frequency.  
15 *Earth and Planetary Science Letters*, 107(3-4): 437-447.
- 16 Lee, S., 1983. A study of the time-averaged palaeomagnetic field for the last 195 million  
17 years. Ph.D. Thesis, Australian National University, Canberra.
- 18 Lovlie, R., 1988. Evidence for Deuteric Magnetization in Hydrothermally Altered  
19 Mesozoic Basaltic Rocks from East Antarctica. *Physics of the Earth and Planetary*  
20 *Interiors*, 52(3-4): 352-364.
- 21 May, S.R., Butler, R.F., Shafiqullah, M. and Damon, P.E., 1986. Paleomagnetism of  
22 Jurassic volcanic rocks in the Patagonia mountains, southeastern Arizona:  
23 implications for the North American 170 Ma reference pole. *Journal of*  
24 *Geophysical Research*, 91: 11545-11555.
- 25 McElhinny, M.W. and McFadden, P.L., 1997. Palaeosecular variation over the past 5  
26 Myr based on a new generalized database. *Geophysical Journal International*,  
27 131(2): 240-252.
- 28 McFadden, P.L. and Merrill, R.T., 1993. Inhibition and Geomagnetic-Field Reversals.  
29 *Journal of Geophysical Research-Solid Earth*, 98(B4): 6189-6199.
- 30 McFadden, P.L., Merrill, R.T. and McElhinny, M.W., 1988. Dipole Quadrupole Family  
31 Modeling of Paleosecular Variation. *Journal of Geophysical Research-Solid Earth*  
32 *and Planets*, 93(B10): 11583-11588.
- 33 McFadden, P.L., Merrill, R.T., McElhinny, M.W. and Lee, S.H., 1991. Reversals of the  
34 Earths Magnetic-Field and Temporal Variations of the Dynamo Families. *Journal*  
35 *of Geophysical Research-Solid Earth and Planets*, 96(B3): 3923-3933.
- 36 McWilliams, M.O. and Howell, D.G., 1982. Exotic terranes of western California.  
37 *Nature*, 297: 215-217.
- 38 Merrill, R.T. and McFadden, P.L., 2003. The geomagnetic axial dipole field assumption.  
39 *Physics of the Earth and Planetary Interiors*, 139(3-4): 171-185.
- 40 Montes-Lauar, C.R. et al., 1994. The Anari and Tapirapua-Jurassic Formations, Western  
41 Brazil - Paleomagnetism, Geochemistry and Geochronology. *Earth and Planetary*  
42 *Science Letters*, 128(3-4): 357-371.
- 43 Mubroto, B., Briden, J.C., McClelland, E. and Hall, R., 1994. Paleomagnetism of the  
44 Balantak Ophiolite, Sulawesi. *Earth and Planetary Science Letters*, 125(1-4): 193-  
45 209.

- 1 Ogg, J.G., 2004. The Jurassic Period. In: F.M. Gradstein, J.G. Ogg and A.G. Smith  
2 (Editors), A geological time scale 2004. Cambridge University Press, Cambridge,  
3 pp. 307-339.
- 4 Ogg, J.G. and Smith, A.G., 2004. The geomagnetic polarity time scale. In: F.M.  
5 Gradstein, J.G. Ogg and A.G. Smith (Editors), A geological time scale 2004.  
6 Cambridge University Press, Cambridge, pp. 63-86.
- 7 Oliver, P.J., Mumme, T.C., Grindley, G.W. and Vella, P., 1979. Paleomagnetism of the  
8 upper Cretaceous Mount Somers Volcanics, Canterbury, New Zealand. New  
9 Zealand Journal of Geology and Geophysics, 22: 199-212.
- 10 Opdyke, N.D. and Channell, J.E.T., 1996. Magnetic Stratigraphy. Academic Press,  
11 London, 346 pp.
- 12 Palmer, H.C., Hayatsu, A. and MacDonald, W.D., 1980. The middle Jurassic Camarca  
13 Formation, Arica, Chile: palaeomagnetism, K-Ar age dating and tectonic  
14 implications. Geophysical Journal of the Royal Astronomical Society, 62: 155-  
15 172.
- 16 Prevot, M., Derder, M.E., McWilliams, M. and Thompson, J., 1990. Intensity of the  
17 Earths Magnetic-Field - Evidence for a Mesozoic Dipole Low. Earth and  
18 Planetary Science Letters, 97(1-2): 129-139.
- 19 Riisager, J., Perrin, M., Riisager, P. and Vandamme, D., 2001. Palaeomagnetic results  
20 and palaeointensity of Late Cretaceous Madagascan basalt. Journal of African  
21 Earth Sciences, 32(3): 503-518.
- 22 Ron, H., Nur, A. and Hofstetter, A., 1990. Late Cenozoic and recent strike slip tectonics in  
23 Mt. Carmel, Northern Israel. Annales Tectonicae, 4(70-80).
- 24 Schult, A., Hussain, A.G. and Soffel, H.C., 1981. Paleomagnetism of upper Cretaceous  
25 volcanics and Nubian Sandstones of Wadi Natash, SE Egypt and implications for  
26 the polar wander path for Africa in the Mesozoic. Journal of Geophysics, 50: 16-  
27 22.
- 28 Smirnov, A.V. and Tarduno, J.A., 2004. Secular variation of the Late Archean Early  
29 Proterozoic geodynamo. Geophysical Research Letters, 31(16):  
30 10.1029/2004GL020333.
- 31 Soffel, H.C., 1981. Palaeomagnetism of a Jurassic ophiolite series in east Elba (Italy).  
32 Journal of Geophysics, 49: 1-10.
- 33 Tarduno, J.A., Cottrell, R.D. and Smirnov, A.V., 2001. High geomagnetic intensity  
34 during the Mid-Cretaceous from Thellier analyses of single plagioclase crystals.  
35 Science, 293(5530): 607-607.
- 36 Tarduno, J.A., Cottrell, R.D. and Smirnov, A.V., 2002. The Cretaceous superchron  
37 geodynamo: Observations near the tangent cylinder. Proceedings of the National  
38 Academy of Sciences of the United States of America, 99(22): 14020-14025.
- 39 Tarduno, J.A. et al., 2003. The Emperor Seamounts: Southward motion of the Hawaiian  
40 hotspot plume in earth's mantle. Science, 301(5636): 1064-1069.
- 41 Tauxe, L. and Staudigel, H., 2004. Strength of the geomagnetic field in the Cretaceous  
42 Normal Superchron: New data from submarine basaltic glass of the Troodos  
43 Ophiolite. Geochemistry Geophysics Geosystems, 5: Art. No. Q02H06.
- 44 Thomas, D.N., Biggin, A.J. and Schmidt, P.W., 2000. A palaeomagnetic study of Jurassic  
45 intrusives from southern New South Wales: further evidence for a pre-Cenozoic  
46 dipole low. Geophysical Journal International, 140(3): 621-635.

- 1 van Dongen, P.G., van der Voo, R. and Raven, T., 1967. Paleomagnetic research in the  
 2 Central Lebanon Mountains and in the Tartous area (Syria). *Tectonophysics*, 4:  
 3 35-53.
- 4 van Hinsbergen, D.J.J., Straathof, G.B., Kuiper, K.F., Cunningham, W.D. and Wijbrans,  
 5 J., 2008. No vertical axis rotations during Neogene transpressional orogeny in the  
 6 NE Gobi Altai: coinciding Mongolian and Eurasian early Cretaceous apparent  
 7 polar wander paths. *Geophysical Journal International*, 173: 105-126.
- 8 Vandall, T.A. and Palmer, H.C., 1990. Canadian Cordilleran Displacement -  
 9 Paleomagnetic Results from the Early Jurassic Hazelton Group, Terrane-I,  
 10 British-Columbia, Canada. *Geophysical Journal International*, 103(3): 609-619.
- 11 Vandamme, D., 1994. A New Method to Determine Paleosecular Variation. *Physics of*  
 12 *the Earth and Planetary Interiors*, 85(1-2): 131-142.
- 13 Vizan, H., 1998. Paleomagnetism of the Lower Jurassic Lepa and Osta Arena formations,  
 14 Argentine Patagonia. *Journal of South American Earth Sciences*, 11(4): 333-350.
- 15 Watson, G.S. and Beran, R.J., 1967. Testing a sequence of unit vectors for serial  
 16 correlation. *Journal of Geophysical Research*, 72: 5655-5659.
- 17 Zhao, X.X., Coe, R.S., Zhou, Y.X., Wu, H.R. and Wang, J., 1990. New Paleomagnetic  
 18 Results from Northern China - Collision and Suturing with Siberia and  
 19 Kazakhstan. *Tectonophysics*, 181(1-4): 43-81.

## 22 **Figure Captions**

23 **Figure 1:** Comparison of VGP dispersion curves (averaged for N and S hemispheres)  
 24 produced by numerical simulations of the geodynamo. The reversing (non-reversing)  
 25 state relates to Model G (Model E) of Glatzmaier et al (1999). A total of 20 kyr of model  
 26 time was used to produce the curves and at each time step (48 years for Model G, 95  
 27 years for Model E), an “instantaneous” VGP dispersion curve was calculated using 72  
 28 “sites” spaced every 5° of longitude along a line of latitude. The circles are the average of  
 29 these instantaneous curves and the error bars represent the standard deviation. The lines  
 30 in (b) are individual “instantaneous” VGP dispersion curves plotted from the *gufm1*  
 31 model (1800-1900; Jackson et al., 2000) and the International Geomagnetic Reference  
 32 Field (IGRF; 1900-2005).

33

1 **Figure 2:** Tests for artefacts introduced by measurement of a VGP dispersion curve using  
2 simulated data. The number of simulated sites ( $N$ ) at each latitude was 1000 in all plots.  
3 Extreme values of the within-site precision parameter ( $\kappa$ ) and number of specimens per  
4 site ( $n$ ) were chosen to show the full range of behaviour. In all cases, the geomagnetic  
5 variation produces Fisher-distributed VGPs with  $S_B = 15^\circ$  at all latitudes (dashed line in  
6 figures). Deviations from this line are purely a product of simulated measurement errors.  
7 No VGP cutoff was applied.

8

9 **Figure 3:** More tests for artefacts introduced by measurement of a VGP dispersion curve  
10 using simulated data.  $N = 1000$  at all latitudes and the within-site precision parameter ( $\kappa$ )  
11 of the simulated data was 182. Unless stated otherwise, a VGP cutoff of  $45^\circ$  was applied.  
12 In plots (a) and (b), the within-site correction was based on the measured estimate ( $k$ ) of  
13 the precision parameter. In plots (c) and (d), the correction was based on a ‘guess’ of the  
14  $k$  value ( $k_{est}$ ) as indicated.

15

16 **Figure 4:** (a) Log-distribution of  $k$  values observed for site means used in this study with  
17  $n \geq 5$ . A normal curve is overlain (b) 10,000 random picks from a distribution modelled  
18 on that observed in (a). (c, d) Simulated VGP dispersion curves ( $N = 1000$  at all latitudes)  
19 produced using site mean data with  $n = 1$  and  $k$  drawn randomly from the distribution  
20 shown in (b). A  $45^\circ$  VGP cutoff was used

21

22 **Figure 5:** Simulated VGP dispersion curves showing the degree of noise introduced by  
23 having different values of  $N$  (number of sites at each latitude). Plotted points are the

1 average of ten separate simulations and the error bars show the full range of the ten  
2 values. The simulated geomagnetic scatter was  $15^\circ$  in the first 7 panels and the individual  
3 sites had  $n = 5$  and  $\kappa = 182$ . No VGP cutoff was applied. Note that a lower geomagnetic  
4 dispersion (last panel) results in less noise being produced (for a given value of  $N$ ).  $\Delta 95$  is  
5 the percentage of the  $S_B$  estimates which are within their associated 95% uncertainty  
6 limits (obtained using the bootstrap approach) of the true value.

7

8 **Figure 6:** Equal area plots showing the locality mean directions (and 95% confidence  
9 circles) for the Gobi Altai lavas used in this study. See table 1 and van Hinsbergen et al  
10 (2008) for more details.

11

12 **Figure 7:** Results from Group 1 ('high quality') Datasets. (a, b): the effects of three  
13 different cutoffs are shown. (c,d) the palaeolatitudes of the datasets are normalised and  
14 the size of each point relates to the size of  $N$  (a few examples are given). The shape  
15 parameters of the best-fit Model G (McFadden et al, 1988) are given with 95% bootstrap  
16 uncertainty limits and the resulting curves plotted. The dashed point in panel (d) was  
17 excluded from the Model G calculation (see text).

18

19 **Figure 8:** Results from Group 2 ('low quality') Datasets. See figure 7 caption for more  
20 information

21

22 **Figure 9:** Results from the study of PSV in the last 5 Myr performed by Johnson et al  
23 (2008; data were taken from their tables 6 and 7). The palaeolatitudes of the datasets are

1 normalised and the size of each point relates to the size of  $N$ . The shape parameters of the  
2 best-fit Model G (McFadden et al, 1988) are given with 95% bootstrap uncertainty limits  
3 and the resulting curves plotted.

4

5 **Figure 10:** VGP dispersion curves using binned data calculated using equation (5).  
6 Uncertainty limits were obtained by applying the same calculation to the upper and lower  
7 95% confidence limits of the individual datasets. The dashed line shows the binned data  
8 of Johnson et al. (2008) for the last 5 Myr (same as figure 9). The number of site mean  
9 data in each bin is given.

10

11 **Figure 11:** The relationship between average reversal frequency and VGP dispersion  
12 curve shape. The ratio  $b/a$  refers to the shape parameters of the best-fit Model G  
13 (McFadden et al., 1988). Diamonds represent the Group1 model fits shown in figure 7  
14 and figure 9 and the thick line is a linear regression fit to these three points. Unfilled  
15 circles represent the curves fitted by McFadden et al (1991) to six different periods in the  
16 last 195 Myr; the dashed line is a linear regression fit to these.

17

18 **Figure 12:** VGP dispersion curves produced using simulated data treated using the same  
19 method as McFadden et al (1991 – filled circles) showing that their  $S_W$  correction  
20 introduces a latitudinal dependence to the plot. The true dispersion is shown by the  
21 dashed line, In all cases  $N = 1000$ ,  $n = 2$ , and  $\kappa = 60$ . In (c), the measured dispersions are  
22 entirely below the simulated values on account of the VGP cutoff ( $40^\circ$ ) employed.

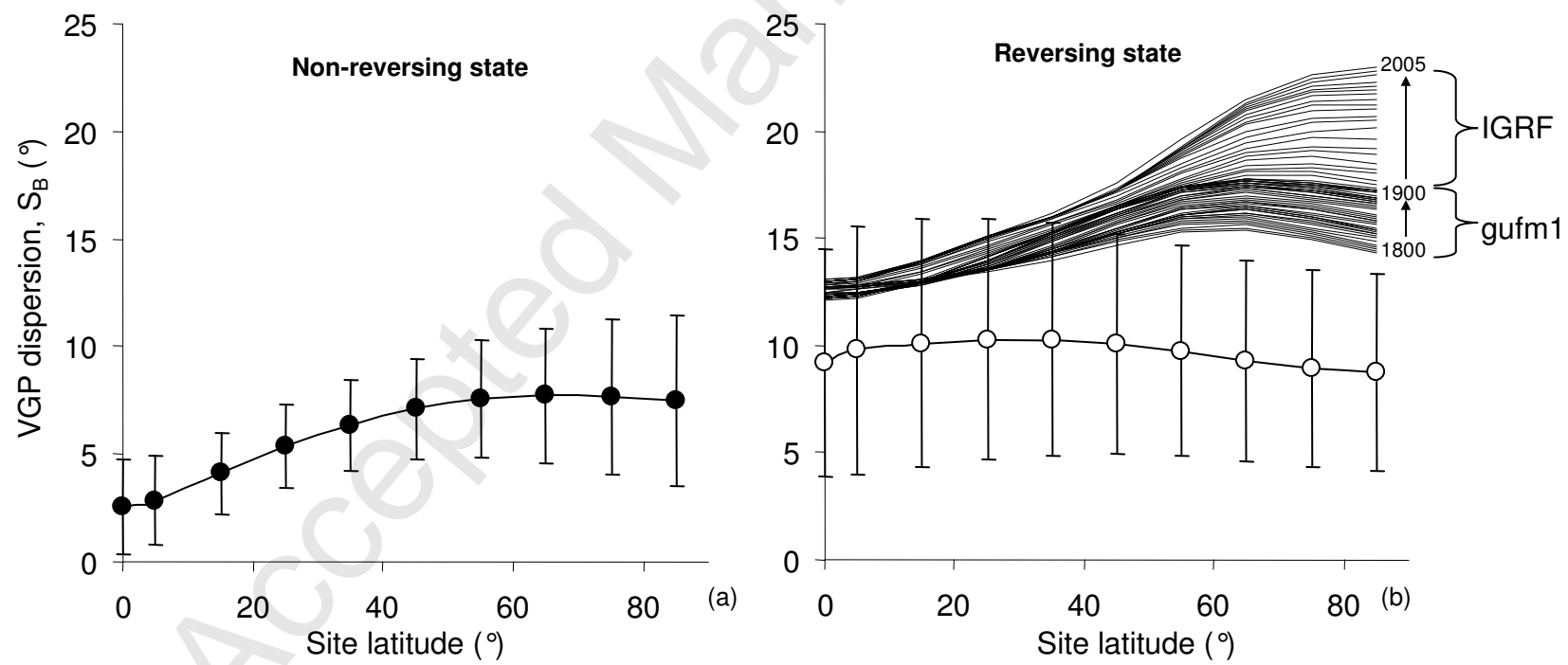


Figure 1

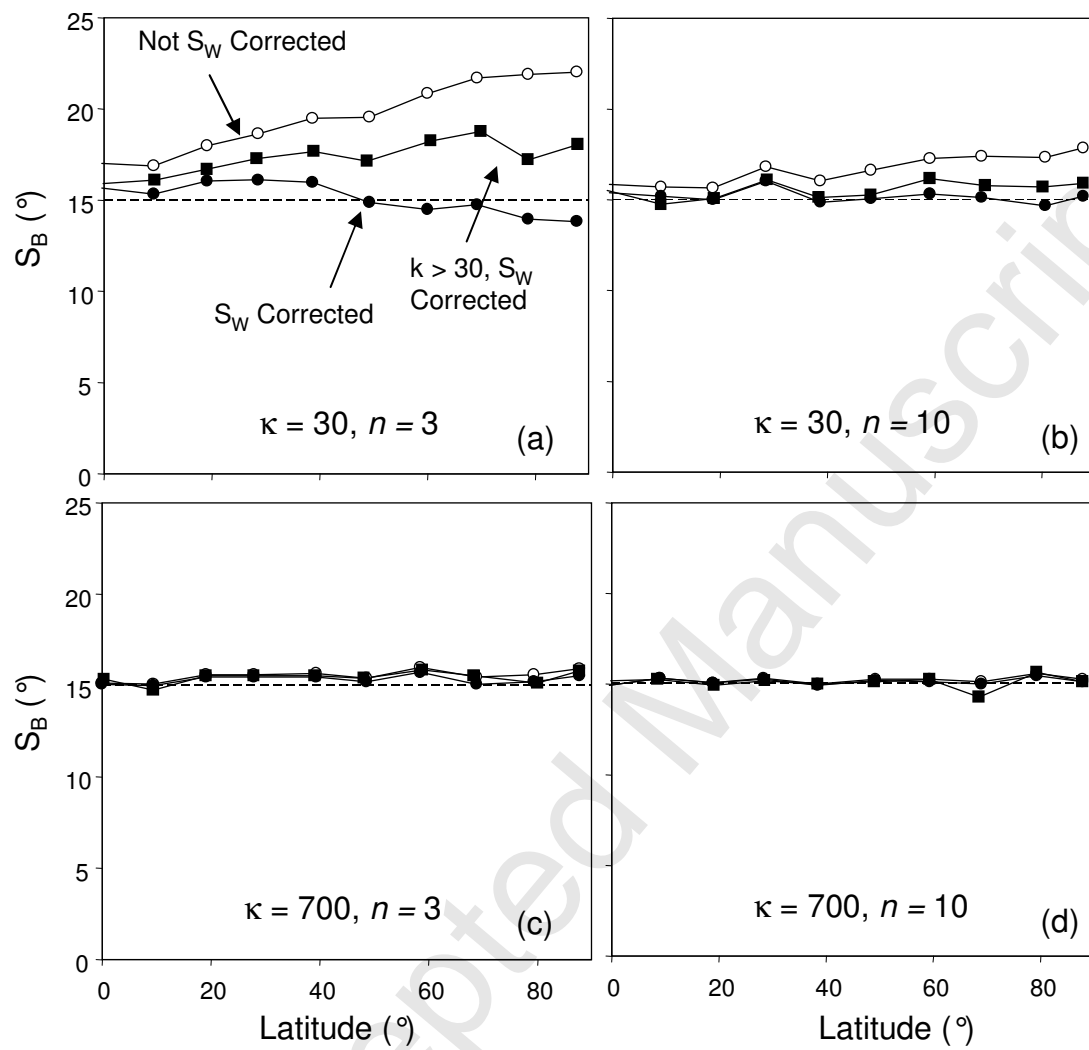


Figure 2

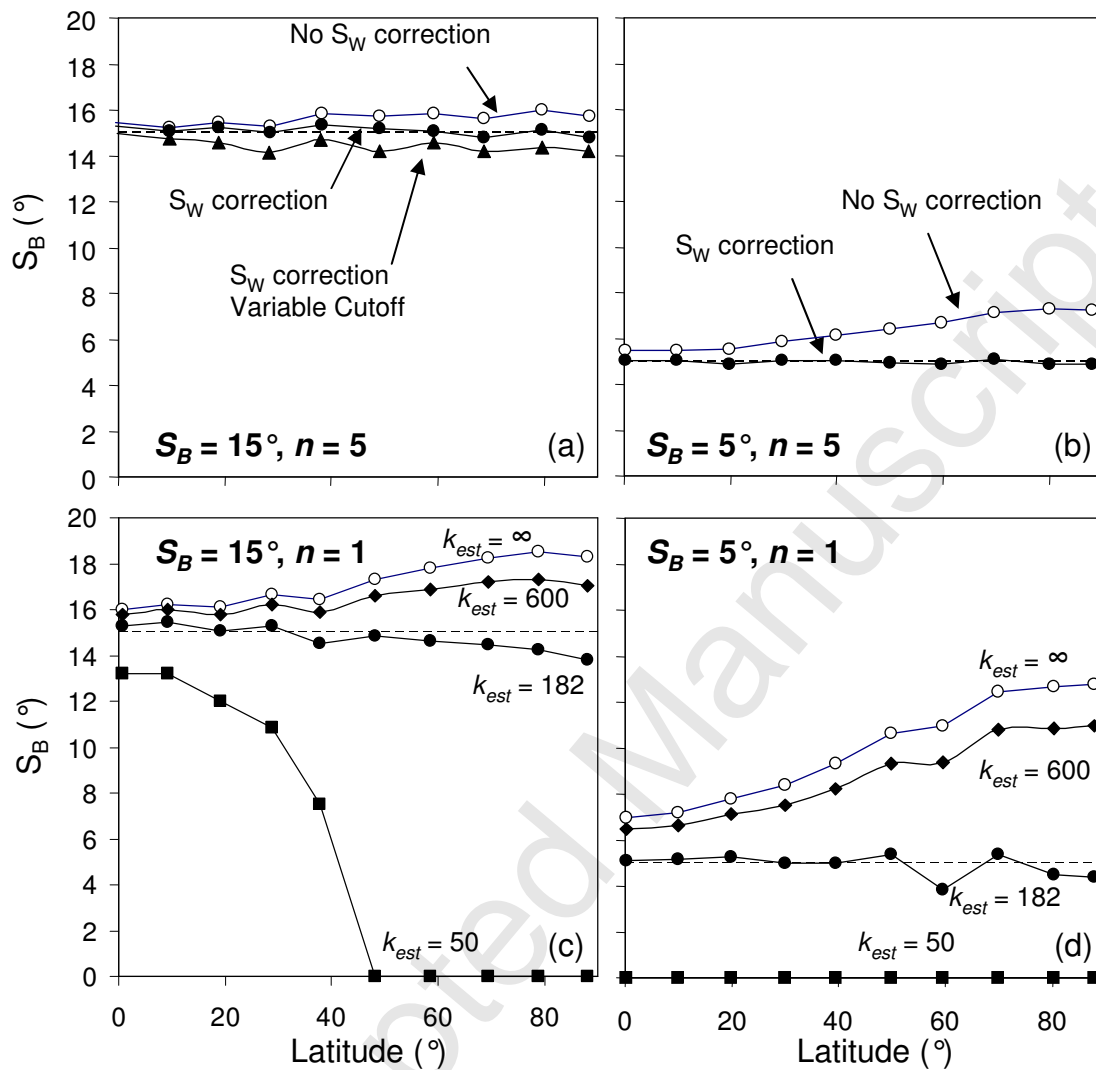


Figure 3

Figure 4

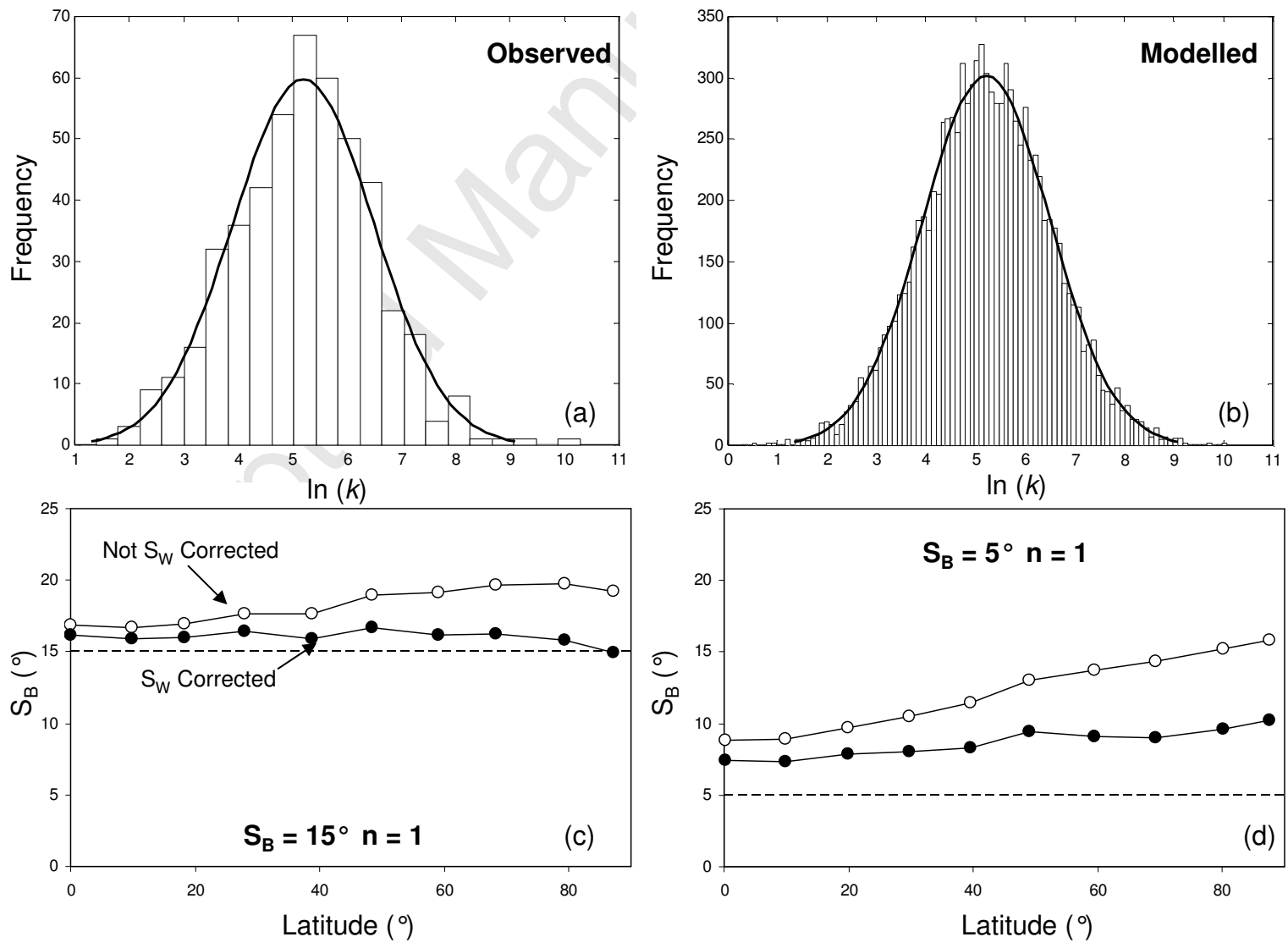


Figure 4

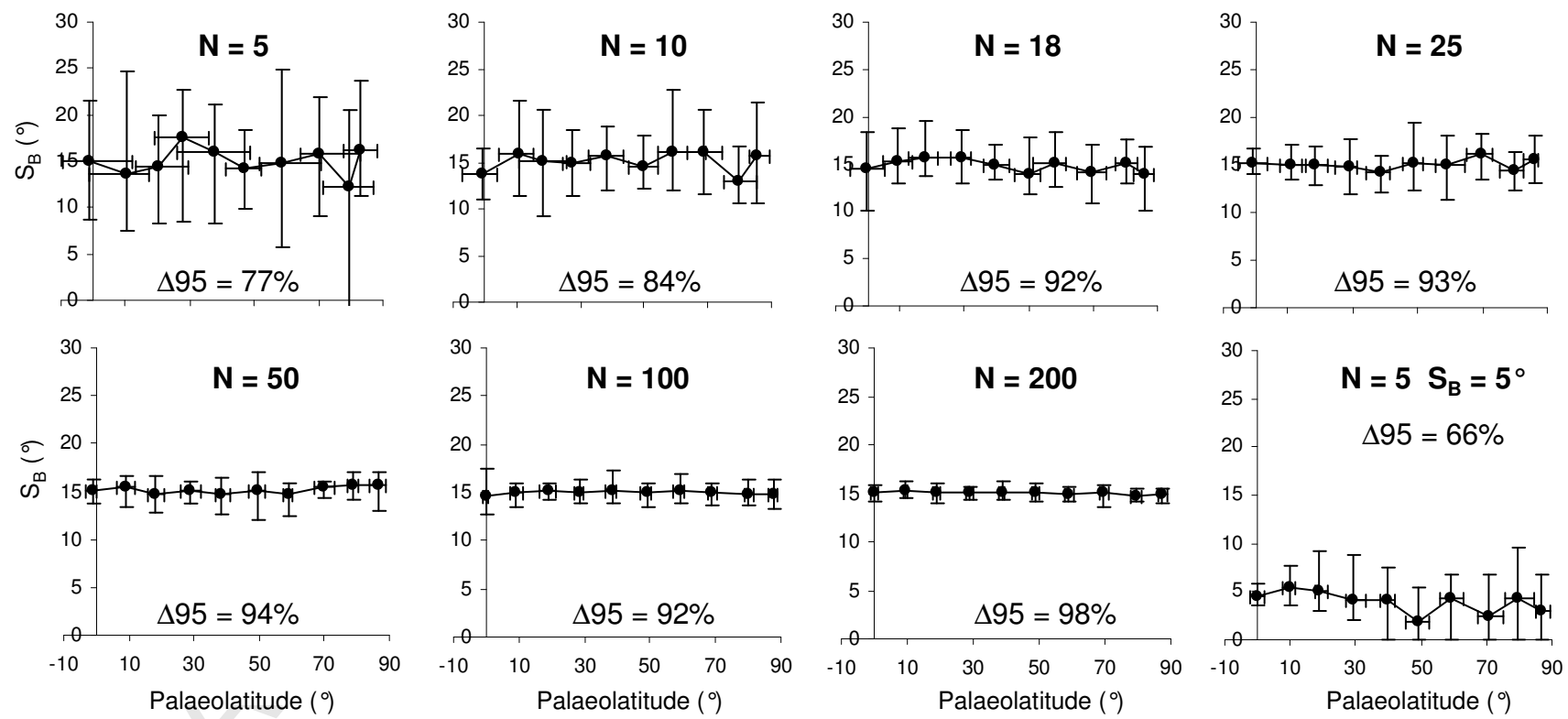


Figure 5

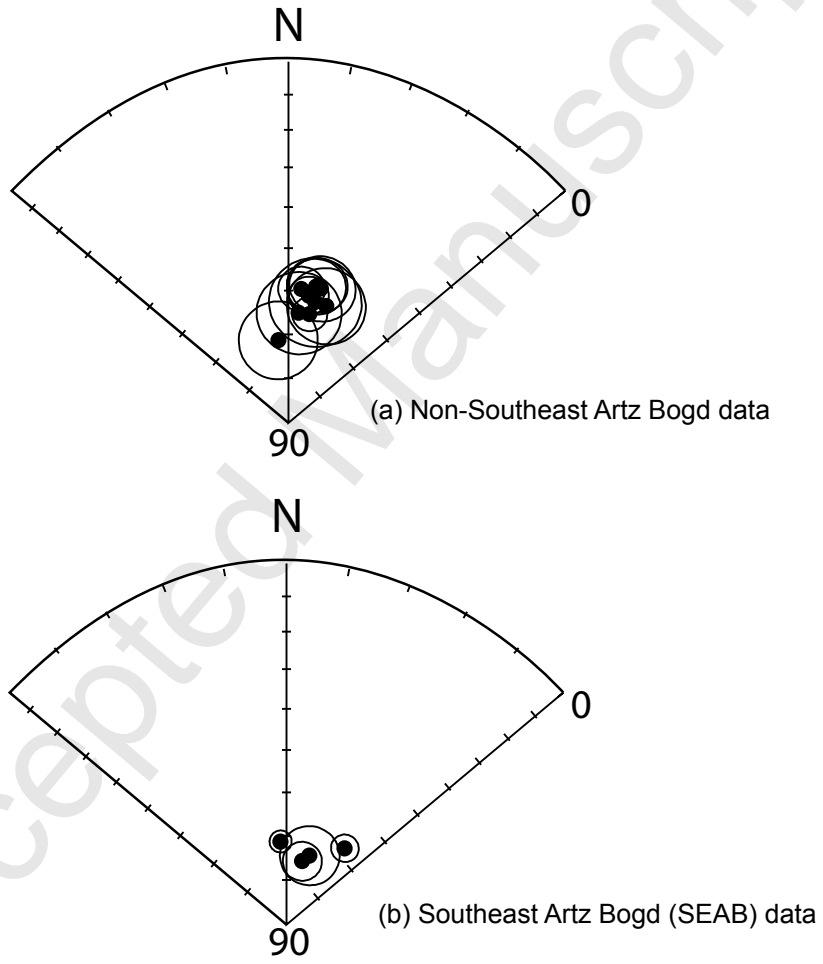


Figure 6:

Figure 7

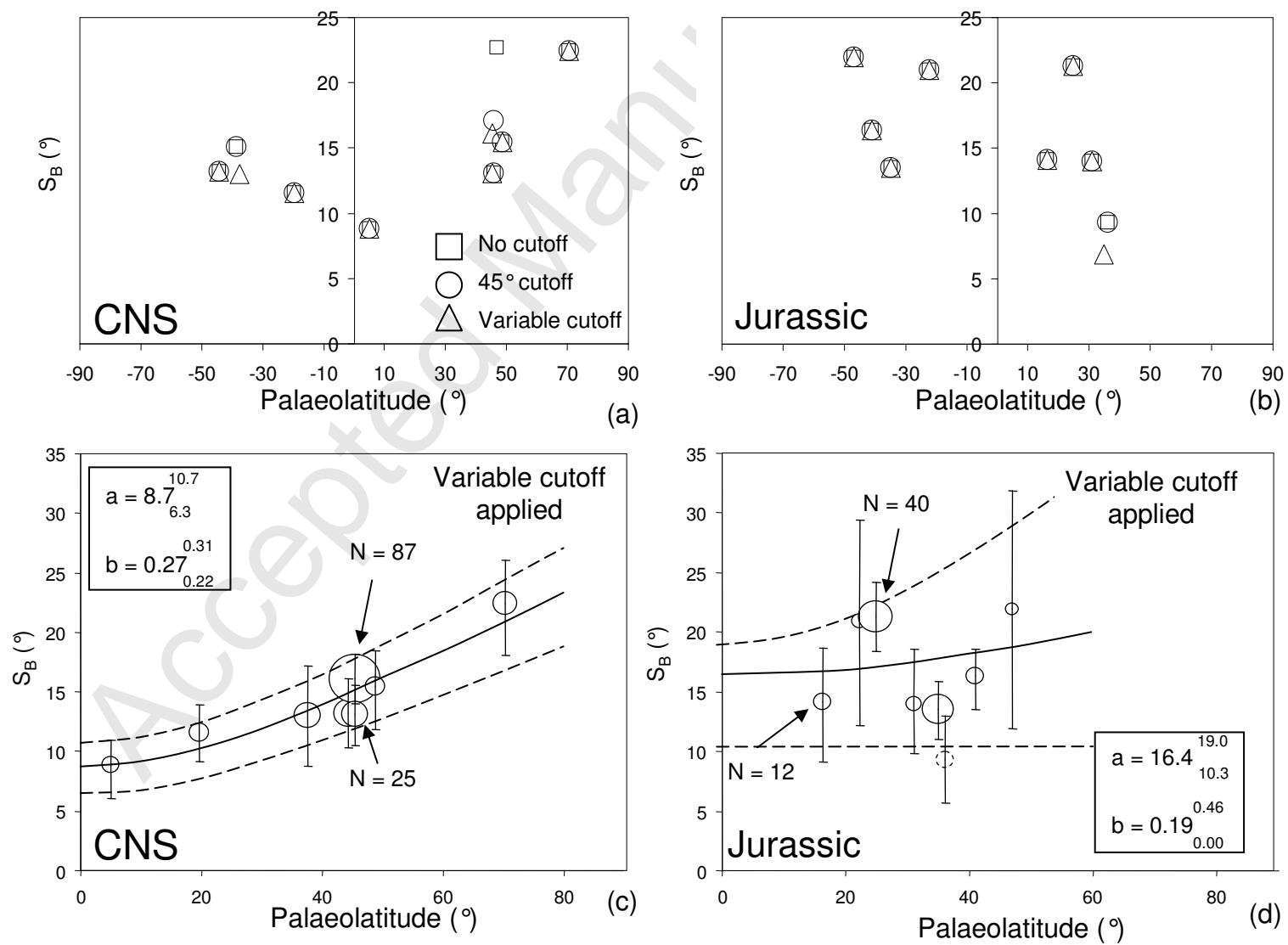


Figure 7

Figure 8

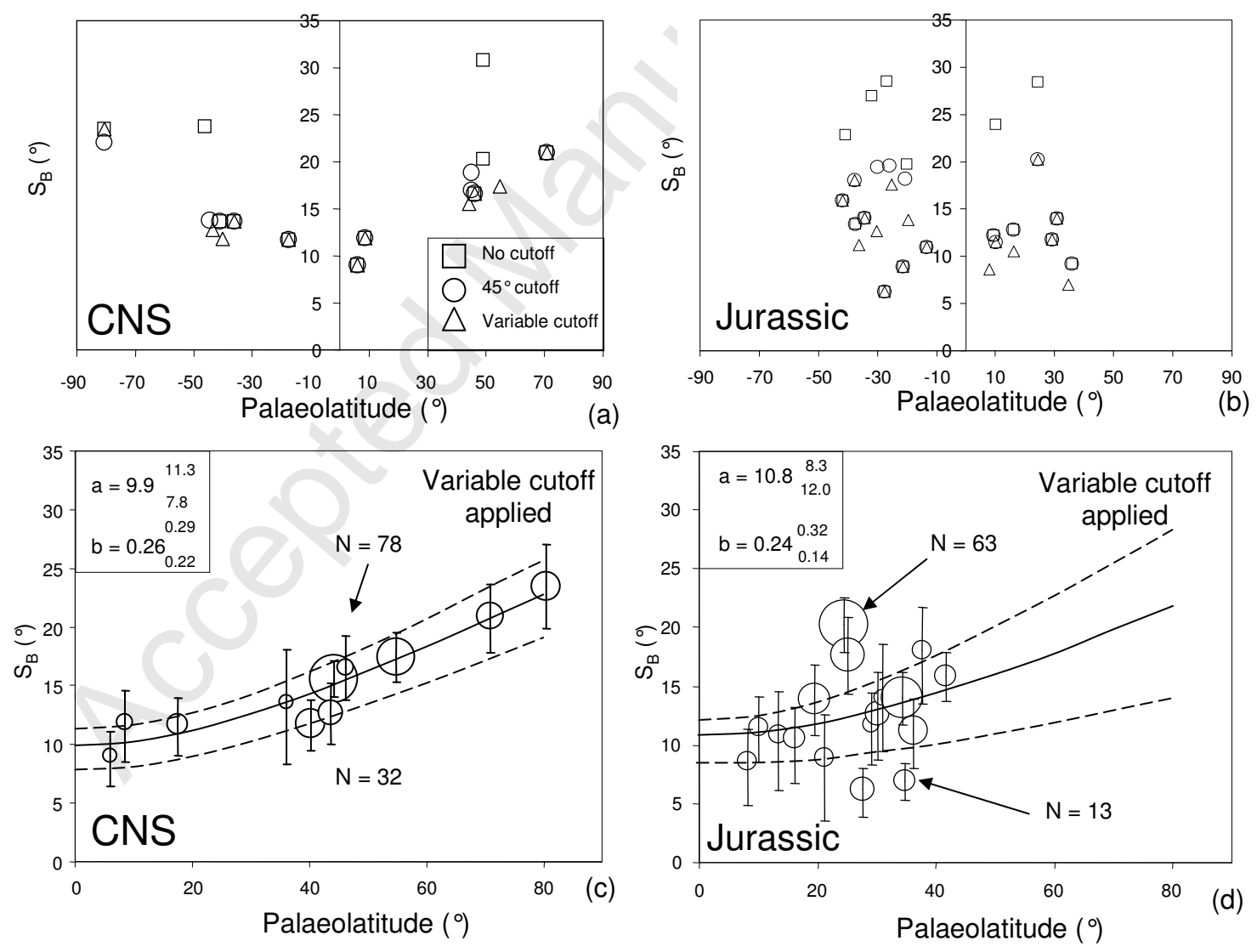


Figure 8

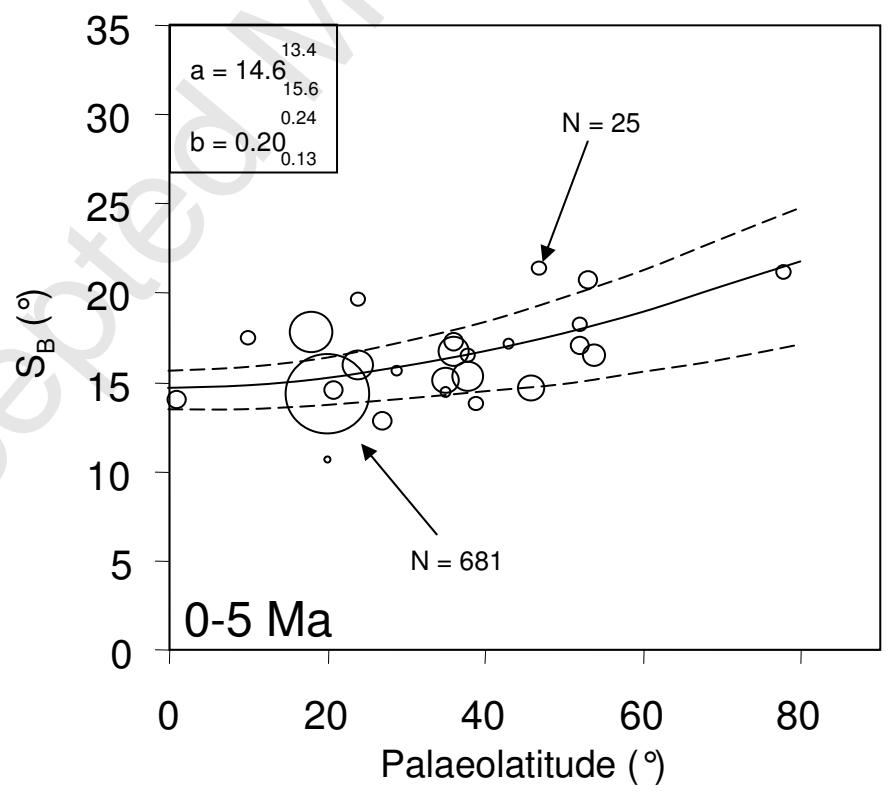


Figure 9

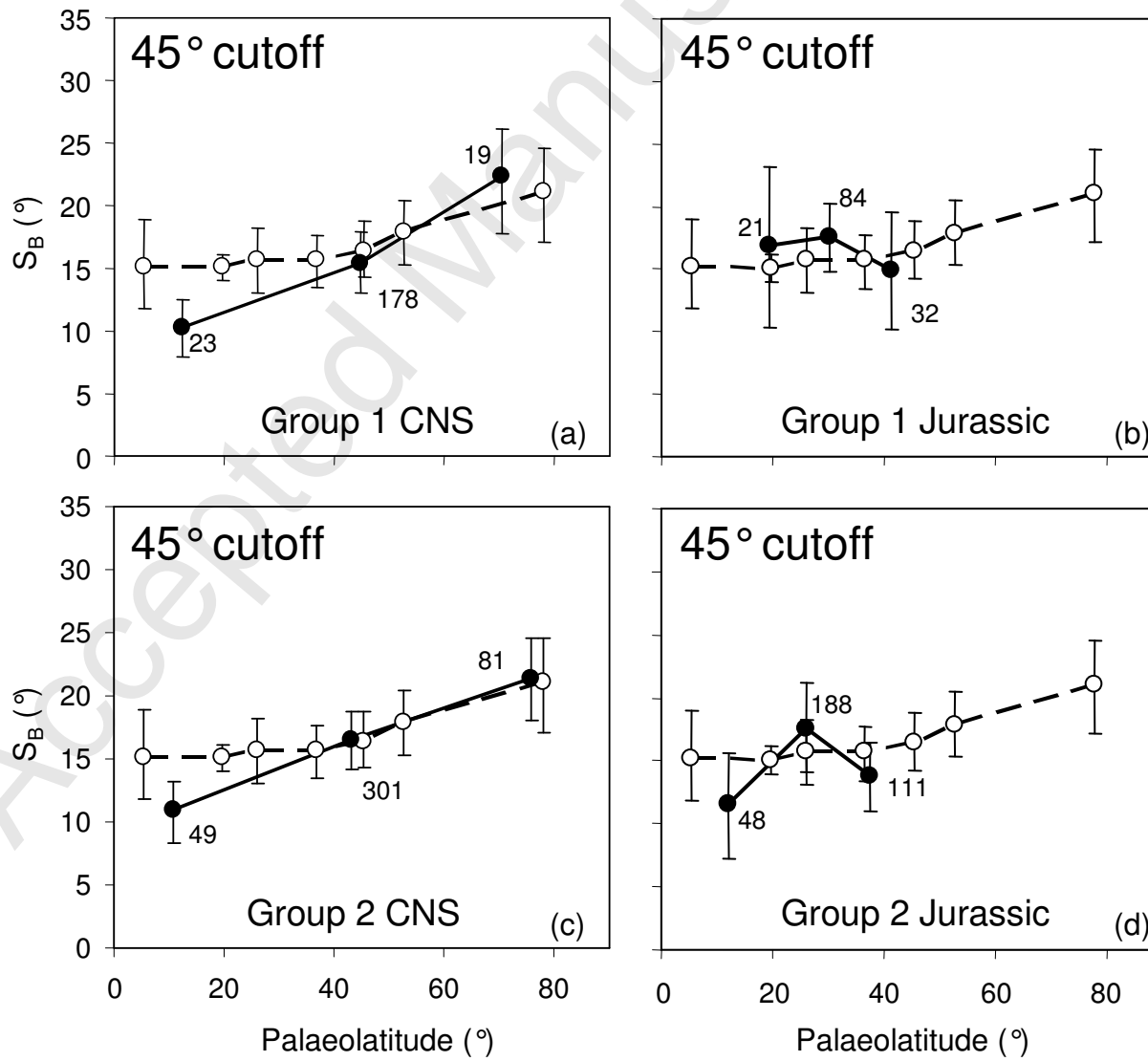


Figure 10

Accepted Manuscript

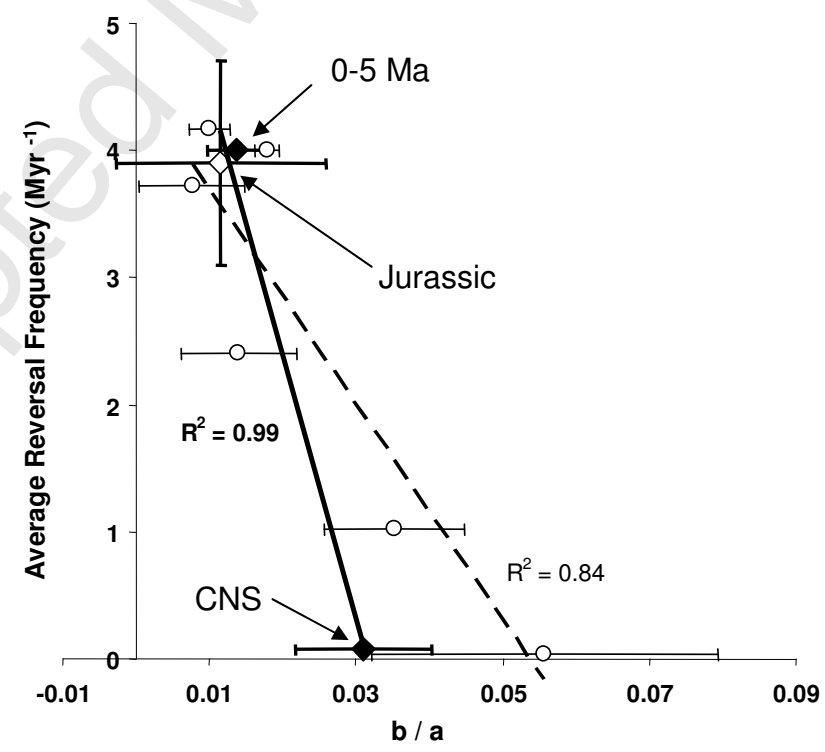


Figure 11

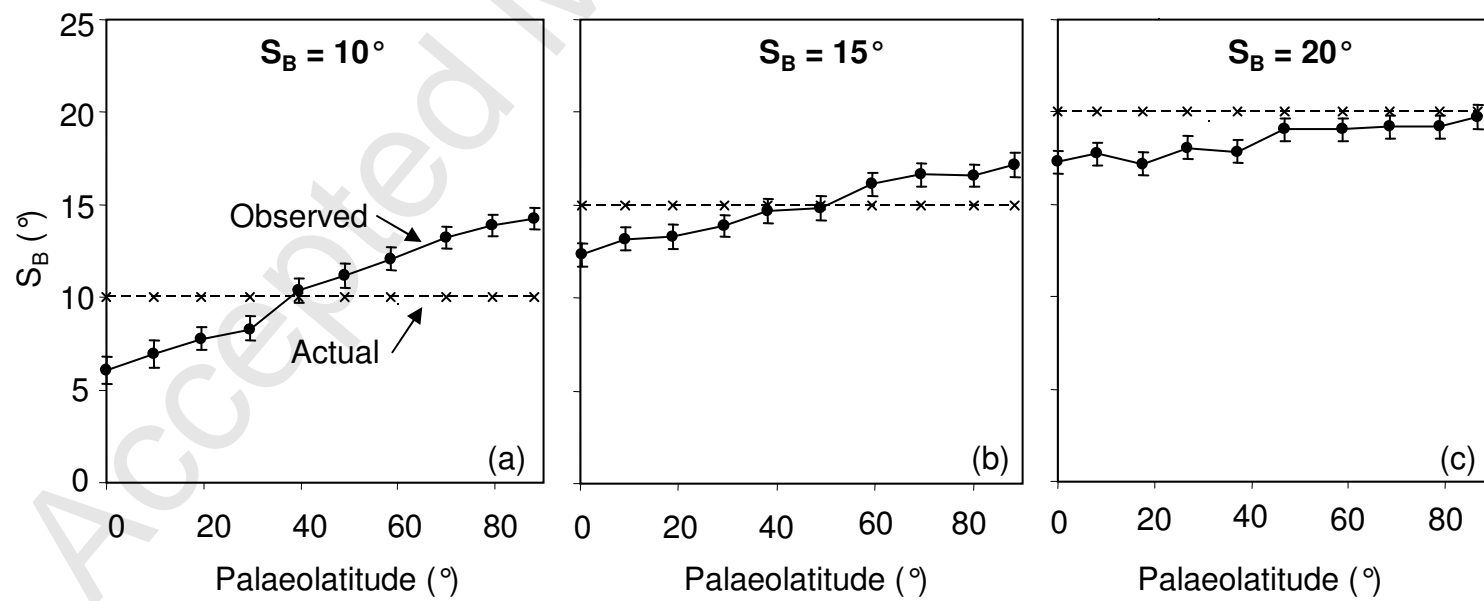


Figure 12

Table 1

Group	Locality	Age (Ma)	Ref.	Lat (°N)	Long (°E)	Dec°	Inc°	N	k	$\alpha_{95}^{\circ}$	NRO factor
SEAB	Kharaat Uul Single Samples	115.4-119.3	This study	44.3	102.7	37.4	68.3	54	42.9	3.1	0.84
SEAB	Tsagaan Tsav	115.4-119.3	vH08	44.4	102.4	13.8	75.3	10	122.2	4.4	0.88
SEAB	Kharaat Uul Multi-samples	115.4-119.3	vH08	44.4	102.6	355.8	71.2	7	597.8	2.5	0.98
SEAB	Khatavch	115.4-119.3	vH08	44.3	102.4	18.4	73.6	9	60.3	6.7	0.41
non-SEAB	Jaran Bogd multi-samples	118.2-124.3	vH08	44.8	100.7	6.4	60.6	16	54.0	5.2	0.99*
non-SEAB	Jaran Bogd 2-samples	118.2-124.3	This study	44.8	100.7	13.5	59.1	14	57.2	6.4	0.26
non-SEAB	Dulaan Bogd	118.2-124.3	vH08	44.9	101.0	12.7	59.5	7	87.6	6.5	
non-SEAB	Baga Bogd	122.7-124.7	vH08	44.8	101.8	14.9	59.7	7	64.3	7.6	0.72
non-SEAB	Bulgantiin Uul	122.7-124.7	vH08	44.8	102.0	19.5	63.2	11	27.7	8.8	0.95*
non-SEAB	Bulgantiin North	122.7-124.7	vH08	44.8	102.0	13.8	63.1	7	35.4	10.3	0.83
non-SEAB	Khalzan Khairkhan	122.7-124.7	vH08	44.7	102.1	353.2	72.5	6	57.5	8.9	0.99
non-SEAB	Tsost	94.7-107	vH08	44.3	102.2	6.5	66.2	7	41.7	9.5	0.34
non-SEAB	Artz Bogd	94.7-107	H05	44.3	102.2	12.4	66.1	30	53.2	3.9	0.99
non-SEAB	Shovon/Khurmen Uul	94.7-107	H05, H07	44.4	103.8	10.2	61.9	24	50.6	4.4	0.52
SEAB	All	115.4-119.3				29.6	70.6	80	44.9	2.5	
non-SEAB	All	94.7-124.7				11.4	62.8	129	49.6	1.9	

**Table 1:** Data from the Gobi Altai basalts used in this study. Refs: vH08 = van Hinsbergen et al (2008); H05 = Hankard et al. (2005); H07 = Hankard et al. (2007). Where several profiles existed within the same locality, the lowest NRO factor (where  $N \geq 5$ ) is given. The asterisk indicates that sedimentary layers had formed between some of the lavas included in the marked profile.

Table 2

Period	Name	Ref	Age (Ma)	Rock type	Demag code	Dec°	Inc°	N	N <sub>0</sub>	NRO factor 1	NRO factor 2	Cutoff°	Δmax°	R	k	α95°	λ	S <sub>l</sub> °	S <sub>B</sub> °	S <sub>u</sub> °
CNS	Rajmahal Traps, India*	[1,2]	113-116	Flood basalts	4,3	312.9	-62.8	27	27	0.93	0.96	28.8	26.7	26.6	66.2	3.4	-44.3	10.4	13.2	15.8
CNS	Madagascar	[3]	84-90	Basalt lavas	4	356.9	-57.1	24	23	0.99	0.62	28.4	27.9	22.7	68.3	3.7	-37.7	9.9	13.0	16.0
CNS	Balantak, Indonesia*	[4]	91-95	Basalt lavas and pillows	4	58.8	-35.6	13	13		0.99	25.9	19.4	12.6	33.5	7.3	-19.7	9.2	11.6	13.7
CNS	Mt Carmel, Israel	[5]	97	Basalt lavas	4	10.4	10.2	10	10			20.9	13.1	9.8	50.8	6.8	5.1	5.9	8.8	11.0
CNS	Gobi Altai non-SEAB	[6,7,8]	95-125	Basalt lavas	4	11.5	63.7	89	85	0.99	0.26	34.0	32.1	83.3	48.8	2.2	45.4	14.3	16.1	17.7
CNS	Spences Bridge, Canada*	[9]	104-105	Andesitic lavas	4	34.3	66.3	13	13	0.97	0.78	32.8	23.3	12.8	58.5	5.5	48.7	12.2	15.4	18.4
CNS	Gobi Altai SEAB*	[6]	115-119	Basalt lavas	4	9.7	73.4	25	25	0.99	0.41	28.5	23.7	24.8	99.8	2.9	45.4 <sup>†</sup>	10.8	13.1	15.2
CNS	Strand Fiord, Canada	[10]	95	Basalt lavas	4	273.8	79.9	19	19	0.97	0.18	45.4	37.7	18.5	39.1	5.4	70.4	17.9	22.4	26.6
Jurassic	Marifil, Argentina	[11]	166-188	Trachi-rhyolites, ignimbrites	4	6.3	-64.9	7	7	0.45		44.5	41.3	6.8	33.1	10.6	-46.8	11.4	22.0	32.2
Jurassic	N El Quemado, Argentina	[11]	154-159	Ignimbrites, rhyolite	4	5.7	-60.0	12	12	0.93	0.86	34.4	21.1	11.8	44.1	6.6	-40.9	13.5	16.4	18.6
Jurassic	Lesotho, S Africa*	[12]	175-185	Basalt lavas	4	339.3	-54.4	35	35	0.99	0.99	29.3	28.4	34.3	47.5	3.6	-34.9	11.2	13.5	15.8
Jurassic	Camaraca, Chile	[13]	157-174	Andesites	3	344.3	-39.2	9	9	0.54	0.07	42.8	39.1	8.5	15.9	13.3	-22.2	11.9	21.0	29.2
Jurassic	Canelo Hills, Arizona	[14]	149-153	Welded tuffs	3	333.8	30.4	12	12			30.4	27.0	11.6	28.6	8.3	16.3	8.9	14.1	18.7
Jurassic	CAMP, Morocco*	[15]	200	Flood basalts	4	343.5	42.7	40	40	0.99	0.93	43.3	39.2	38.0	19.8	5.2	24.8	18.3	21.3	24.2
Jurassic	Hua-an, Mongolia	[16]	146-166	Andesites, tuff	4	10.1	50.1	9	9	0.91		30.2	26.2	8.8	45.8	7.7	30.9	9.4	14.0	18.7
Jurassic	Manzhouli, Mongolia*	[16]	146-166	Tuffs	4	30.7	54.3	13	12	0.91		17.3	10.4	11.9	179.5	3.2	34.9	5.0	6.9	8.4

**Table 2:** Group 1 datasets. Demag code refers to that used in the Global Palaeomagnetic database (<http://www.ngu.no/dragon/Palmag/paleomag.htm>).  $N_0$  is the number of sites before the VGP cutoff is applied.  $\Delta_{max}$  is the maximum angular distance between a single pole and the mean pole after the cutoff is applied.  $S_l$  and  $S_u$  are the upper and lower 95% confidence limits (obtained by the bootstrap method) on the VGP dispersion  $S_B$ . See text for definition of other parameters. References: [1] Tarduno et al (1971); [2] Klootwijk (1971); [3] Riisager et al. (2001); [4] Mubroto et al. (1994); [5] Ron et al. (1990); [6] van Hinsbergen et al (2008); [7,8] Hankard et al. (2005, 2007); [9] Irving et al. (1990); [10] Tarduno et al. (2002); [11] Iglesia Llanos et al. (2003); [12] Kostrov & Perrin (1996); [13] Palmer et al. (1980); [14] Kluth et al. (1982); [15] Knight et al. (2004); [16] Zhao et al. (1990). \*The reliability of these datasets is discussed explicitly in the text. <sup>†</sup>The palaeolatitude of the Gobi Altai SEAB dataset was manually changed to match that of the Gobi Altai non-SEAB dataset.

Table 3

Period	Name	Ref	Age (Ma)	Rock type	Demag code	Dec°	Inc°	N	N <sub>0</sub>	NRO factor 1	NRO factor 2	Cutoff†	Δmax*	R	k	α95°	λ	S <sub>i</sub> °	S <sub>B</sub> °	S <sub>u</sub> °
CNS	Mt Somers, New Zealand*	[17]	92-98	Intermediate-felsic flows and tuffs	3	353.7	-85.2	46	46	0.94		47.3	46.3	44.6	31.7	3.8	-80.5	19.9	23.5	26.8
CNS	Rajmahal Traps, India*	[1,2]	113-116	Flood basalts	4,3	313.5	-62.3	33	31	0.93	0.96	27.9	27.4	30.6	70.0	3.1	-43.6	10.1	12.7	15.1
CNS	Madagascar	[3]	84-90	Basalt lavas	4	0.3	-59.4	44	42	0.99	0.62	26.2	24.3	41.5	79.7	2.5	-40.2	9.6	11.8	13.8
CNS	Vinita, Chile*	[12]	97-106	Intermediate lavas and tuffs	3	8.0	-55.5	11	11	0.66		29.5	27.4	10.8	55.3	6.2	-36.1	8.0	13.6	18.5
CNS	Balantak, Indonesia*	[4]	91-95	Basalt lavas and pillows	4	59.9	-32.1	23	23		0.99	26.0	21.8	22.3	30.4	5.6	-17.4	9.4	11.7	14.0
CNS	Mt Carmel, Israel	[5]	97	Basalt lavas	4	10.1	11.9	11	11			21.2	13.2	10.8	43.8	7.0	6.0	6.4	9.0	10.8
CNS	Wadi Natash, Egypt	[18]	86-100	Mafic to felsic lava flows	3	345.4	16.7	15	15			26.4	19.7	14.3	21.4	8.5	8.5	8.7	11.9	14.7
CNS	Gobi Altai non-SEAB	[6,7,8]	95-125	Basalt lavas	4	11.4	62.8	129	116	0.99	0.26	33.0	32.0	113.7	49.6	1.9	44.2	14.1	15.6	17.0
CNS	Spences Bridge, Canada*	[9]	104-105	Andesitic lavas	4	38.5	64.4	16	16	0.97	0.78	34.8	23.5	15.6	42.5	5.7	46.2	13.5	16.6	19.2
CNS	Gobi Altai SEAB*	[6]	115-119	Basalt lavas	4	29.6	70.6	80	75	0.99	0.41	36.4	35.6	73.4	44.9	2.5	54.9 <sup>†</sup>	15.4	17.4	19.4
CNS	Strand Fiord, Canada	[10]	95	Basalt lavas	4	284.8	80.1	37	37	0.97	0.18	42.7	37.1	36.2	43.5	3.6	70.8	17.8	20.9	23.9
Jurassic	N El Quemado, Argentina	[11]	154-159	Welded ignimbrites, rhyolite	4	8.9	-60.6	14	14	0.93	0.86	33.7	22.2	13.7	45.3	6.0	-41.6	13.8	15.9	17.9
Jurassic	Marifil, Argentina	[11]	166-188	Trachi-rhyolites, welded ignimbrites	4	2.9	-57.0	11	10	0.45		37.5	26.3	9.7	32.2	8.6	-37.6	13.5	18.0	21.7
Jurassic	Vestfjella, Antarctica*	[19]	152-176	Basaltic lavas and dykes	3	31.7	-55.6	26	24			25.2	25.0	23.6	56.7	4.0	-36.2	8.0	11.2	13.9
Jurassic	Lesotho, South Africa*	[12]	175-185	Basalt flows	4	338.8	-53.8	47	47	0.99	0.99	30.3	28.9	45.9	42.0	3.2	-34.3	11.7	14.1	16.2
Jurassic	Lembobo, South Africa*	[20]	173-183	Basalts & intrusive rhyolites	3	336.3	-49.3	21	17	0.52		27.8	26.3	16.7	49.8	5.1	-30.2	8.7	12.7	16.2
Jurassic	Anari & Tapirapua, Brazil	[21]	195-198	Basalt flows	3	21.2	-46.3	15	15	0.52		16.3	12.1	14.9	103.1	3.8	-27.6	3.9	6.3	8.0
Jurassic	Lepa, Argentina	[22]	182-191	Andesites and tuffs	4	10.3	-43.1	36	30	0.82	0.29	36.7	33.5	28.5	19.9	6.0	-25.1	14.4	17.6	20.9
Jurassic	East Elba Ophiolite, Italy	[23]	146-157	Pillow basalts	3	199.6	-37.9	10	10	0.49		21.1	18.9	9.8	39.4	7.8	-21.2	3.6	8.9	12.6
Jurassic	Camaraca, Chile	[13]	157-174	Andesites	3	336.2	-35.3	32	28	0.54	0.07	30.0	29.8	27.0	27.3	5.3	-19.5	10.8	13.9	16.8
Jurassic	Coast Range Ophiolite, California	[24]	155-165	Pillow basalts	3	40.9	-25.4	10	10			24.7	19.2	9.8	38.2	7.9	-13.3	6.2	11.0	14.5
Jurassic	Lebanon	[25, 26]	146-156	Basalt flows and dykes, 2 tuffs	3	92.2	15.8	12	11			20.5	16.3	10.7	33.4	8.0	8.1	4.8	8.6	11.3
Jurassic	Corral Canyon, Arizona	[27]	166-178	Welded tuffs	4	339.5	19.5	13	11			25.7	17.7	10.7	29.9	8.5	10.0	8.6	11.5	14.1
Jurassic	Canelo Hills, Arizona	[14]	149-153	Welded tuffs	3	337.2	30.1	15	14			24.0	18.6	13.7	41.8	6.2	16.2	6.8	10.6	13.2
Jurassic	CAMP, Morocco*	[15]	200	Flood basalts	4	349.1	42.3	64	63	0.99	0.93	41.5	38.5	60.1	21.3	4.0	24.5	17.9	20.3	22.6
Jurassic	Zymoetz, Canada*	[28]	190-200	Flows, tuffs, ignimbrites	4	226.3	48.1	9	9	0.24		26.2	18.3	8.8	47.5	7.5	29.1	8.3	11.8	14.5
Jurassic	Hua-an, Mongolia	[16]	146-166	Andesites, 1 tuff	4	10.1	50.1	9	9	0.91		30.2	26.2	8.8	45.8	7.7	30.9	9.4	14.0	18.6
Jurassic	Manzhouli, Mongolia*	[16]	146-166	Tuffs	4	31.7	54.2	14	13	0.91		17.6	10.4	12.9	172.2	3.2	34.7	5.3	7.0	8.4

**Table 3:** Group 2 datasets. See table 2 and text for definition of other parameters. References (see also table 2): [17] Oliver et al. (1979); [18] Schult et al. (1981); [19] Lovlie (1988); [20] Henthorn, 1981; [21] Montes-Lauar et al. (1994); [22] Vizán (1998); [23] Soffel (1981); [24] McWilliams & Howell (1982); [25] Gregor et al. (1974); [26] van Dongen et al. (1967); [27] May et al. (1986); [28] Vandall & Palmer (1990). \*The reliability of these datasets is discussed explicitly in the text. †The palaeolatitude of the Gobi Altai SEAB dataset was manually changed to match that of the Gobi Altai non-SEAB dataset.

Flow	Lat (°N)	Long (°E)	Dec°	Inc°	n
<i>Jaran Bogd</i>					
3	44.865	100.738	28.5	64.3	2
4	44.864	100.741	22.3	59.9	2
6	44.862	100.748	7.1	70.5	2
8	44.849	100.749	37.8	63.7	2
9	44.846	100.742	10.4	56.0	2
10	44.845	100.749	194.1	12.4	2
11	44.844	100.743	348.7	55.2	2
12	44.841	100.739	30.8	53.5	2
13	44.837	100.749	236.5	21.7	2
14	44.837	100.748	201.1	62.3	2
15	44.832	100.772	359.1	50.7	2
16	44.748	100.772	355.2	55.4	2
18	44.830	100.773	160.7	68.2	2
19	44.825	100.797	22.1	52.3	2
<i>Kharaat Uul</i>					
KU 50	44.430	102.630	3.4	61.6	1
KU 51	44.429	102.629	353.2	39.3	1
KU 53	44.416	102.626	84.0	64.2	1
KU 55	44.412	102.625	101.8	79.8	1
KU 56	44.406	102.624	79.9	72.6	1
KU 57	44.405	102.623	259.5	84.1	1
KU 65	44.401	102.585	10.7	69.1	1
KU 66	44.399	102.586	70.8	75.4	1
KU 67	44.397	102.585	32.4	72.0	1
KU 68	44.395	102.579	10.8	73.7	1
KU 69	44.393	102.578	21.0	65.3	1
KU 71	44.386	102.581	44.6	67.7	1
KU 72	44.383	102.581	64.9	76.4	1
KU 73	44.377	102.583	53.5	59.2	1
KU 74	44.370	102.623	11.4	47.2	1
KU 75	44.372	102.634	47.8	58.4	1
KU 76	44.372	102.635	67.4	53.6	1
KU 77	44.374	102.648	343.0	67.8	1
KU 78	44.372	102.649	16.7	65.5	1
KU 79	44.371	102.650	47.0	73.0	1
KU 80	44.371	102.650	77.7	58.8	1
KU 81	44.370	102.657	55.9	66.6	1
KU 83	44.368	102.683	27.0	66.4	1
KU 84	44.367	102.684	76.0	57.1	1
KU 85	44.367	102.684	49.3	65.1	1
KU 87	44.365	102.698	32.8	69.7	1
KU 90	44.358	102.705	354.0	67.1	1
KU 92	44.351	102.704	27.3	63.7	1
KU 93	44.350	102.703	15.0	66.3	1
KU 94	44.348	102.703	88.5	78.1	1
KU 95	44.347	102.704	67.1	81.8	1
KU 96	44.344	102.707	50.5	61.6	1
KU 97	44.343	102.808	18.6	64.5	1
KU 98	44.342	102.709	127.6	72.2	1
KU 99	44.339	102.712	5.3	72.1	1
KU 100	44.340	102.716	292.4	80.3	1
KU 101	44.339	102.718	48.3	77.2	1
KU 102	44.339	102.720	34.2	61.7	1
KU 103	44.338	102.728	48.3	53.7	1
KU 104	44.337	102.740	73.9	70.8	1
KU 105	44.337	102.740	36.1	67.5	1
KU 106	44.336	102.741	47.8	60.8	1
KU 107	44.334	102.751	39.0	64.9	1
KU 109	44.331	102.756	102.8	54.6	1
KU 110	44.331	102.758	9.0	64.4	1
KU 111	44.330	102.760	7.9	64.9	1
KU 112	44.330	102.764	28.2	68.6	1
KU 113	44.329	102.766	16.2	63.9	1
KU 115	44.304	102.774	25.7	54.9	1
KU 116	44.302	102.775	17.3	61.3	1
KU 118	44.296	102.773	56.7	71.7	1
KU 119	44.293	102.772	1.5	60.7	1
KU 120	44.292	102.771	52.1	65.4	1
KU 121	44.289	102.774	59.0	67.0	1

**Table A1:** New data used in this study taken from basalt lavas. All directions are tilt-corrected